



Title	Study on the aggregation mechanism of $\beta 2$ -microglobulin focused on amyloid fibrils and amorphous aggregates
Author(s)	足立, 誠幸
Citation	大阪大学, 2018, 博士論文
Version Type	VoR
URL	<a href="https://doi.org/10.18910/69367">https://doi.org/10.18910/69367</a>
rights	
Note	

*The University of Osaka Institutional Knowledge Archive : OUKA*

<https://ir.library.osaka-u.ac.jp/>

The University of Osaka

**Study on the aggregation mechanism of  
 $\beta_2$ -microglobulin focused on  
amyloid fibrils and amorphous aggregates**

(アミロイド線維とアモルファス凝集に着眼した  
 $\beta_2$ ミクログロブリン凝集機構についての研究)

A Doctoral Thesis

by

Masayuki Adachi

Submitted to the Graduate school of Science

Osaka University

February, 2018

## Acknowledgement

This work has been performed under the direction of Professor Yuji Goto (Institute for Protein Research, Osaka University). I would like to express sincere gratitude to his guidance, discussion and encouragement.

I would like to acknowledge Professor Toshimichi Fujiwara (Institute for Protein Research, Osaka University) and Professor Genji Kurisu (Institute for Protein Research, Osaka University) for their accepting this dissertation.

I am deeply indebted to Assistant Professor Masatomo So (Institute for Protein Research, Osaka University) for his valuable discussion, experimental support and helpful advice. I would like to express my great appreciation to Associate Professor Kazumasa Sakurai (Institute of Advanced Technology, Kinki University) for his supports and helpful advice for measurement of analytical ultracentrifuge and analysis those data, and to Associate Professor József Kardos (Eötvös Loránd University) for discussion of my study and measurement of FTIR. I also grateful to Dr. Tatsuya Ikenoue (University of Cambridge) for support and helpful advice for measurement of AFM.

This work was supported by members of Laboratory of Protein Folding, Institute for Protein Research, Osaka University. I am grateful to Lecture Young-Ho Lee, Lecture Kenji Sasahara and Assistant Professor Keiichi Yamaguchi for giving helpful advice. I am also grateful to Mr. Misaki Kinoshita and Mr. Hiroya Muta for many suggestion and discussion without hesitation as classmate, and to Mrs. Kyoko Kigawa, Mrs. Yukiko Moriyama and Mrs. Yuko Kitamura for the assistance of protein expression and purification, and to Mrs. Mmiko Ishii and Mrs. Chizu Sasai for assistance of daily life.

Furthermore, I would like to really thank to members of the Laboratory of Protein Folding for their warmhearted encouragement making me happy every day in the life of Osaka University.

I thank supports form “SUNBOR SCHOLARSHIP” of Suntory Foundation for Life Sciences, and The Research Fellowships of the Japan Society for Promotion of Science for Young Scientists. They give me the opportunity for research in blessed environment.

Finally, I thank sincerely my family for kindness many supports and encouragements.

---

Masayuki Adachi

February 2018

# Contents

<b>Chapter 1. General introduction</b> .....	1
1.1 Protein misfolding and aggregation .....	2
1.2 Amyloid fibrils and amorphous aggregates .....	3
1.3 $\beta_2$ -microglobulin ( $\beta_2m$ ) .....	7
1.4 Outline of this dissertation .....	9
<b>Chapter 2. Supersaturation-limited and unlimited phase transitions compete to produce the pathway complexity in amyloid fibrillation ...</b>	11
2.1 Introduction.....	12
2.2 Materials and methods .....	15
2.3 Results.....	19
2.4 Discussion .....	35
2.5 Conclusion .....	48
<b>Chapter 3. Comprehensive understanding of heat- and salt-dependent protein aggregation based on the supersaturation-limited competitive mechanism</b> .....	50
3.1 Introduction.....	51
3.2 Materials and methods .....	53
3.3 Results.....	56

3.4 Discussion.....	67
3.4 Conclusion .....	74
<b>Chapter 4. General conclusion .....</b>	<b>75</b>
<b>References .....</b>	<b>78</b>
<b>List of publications.....</b>	<b>91</b>

## Abbreviations

A $\beta$	amyloid- $\beta$
$\beta$ 2m	$\beta$ <sub>2</sub> -microglobulin
CD	circular dichroism
ThT	thioflavin T
MHC I	major histocompatibility complex class I
DRA	dialysis-related amyloidosis
ANS	8-anilino-1-naphthalenesulfonic acid
AFM	atomic force microscopy
TEM	transmission electron microscopy
FTIR	fourier transform infrared spectroscopy
ITC	isothermal titration calorimetry
DSC	differential scanning calorimetry
MRE	mean residue ellipticity

## Chapter 1. General introduction

## 1.1 Protein misfolding and aggregation

Proteins are macromolecules of polypeptide chains made of 20 kinds of amino acids, which fold into their specific structures, so-called native structure. Proteins that folded into the native structure play crucial roles in our life. It has been considered that their native structures adopt the thermodynamically most stable state determined by amino acid sequence. By this way of consideration, even if proteins unfold to random structure, they are able to re-fold into the native structure. C. B. Anfinsen considered that a very fine balance exists between the native and random structures<sup>1</sup>. However, proteins sometimes form aggregates which are distinct from the native structure (Fig. 1)<sup>2</sup>. These aggregates are considered to be a misfolded state caused by various factors such as alternations in environments or mutations. Although quality-control mechanisms with chaperones exist, aggregation of proteins is often observed both in and out of cells, causing cell and tissue dysfunctions<sup>3-5</sup>. Here, the aggregates of denatured proteins can be largely classified into two types; amyloid fibrils and amorphous aggregates<sup>6</sup>.

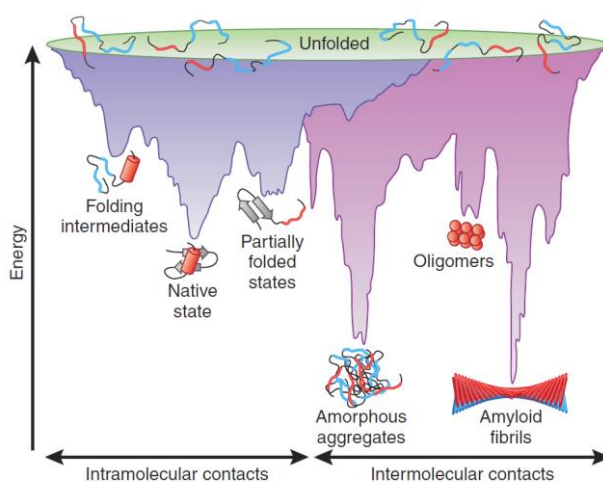


**Figure 1.** Energy landscape scheme of protein folding and aggregation.

Proteins form not only native structure but also some aggregates from unfolded state. This figure is reproduced from Hartl, F. U. et al. 2009 with permission<sup>2</sup>.

## 1.2 Amyloid fibrils and amorphous aggregates

As described above, it has been recognized that there are two types of protein aggregates. Amyloid fibrils have highly ordered cross- $\beta$  structure stabilized by hydrogen bond network and are able to be observed as fibrillar aggregates with a width of approximately 10 nm and length of several micrometers using electron microscopy (EM). The repeating  $\beta$  sheet was characterized by X-ray fiber diffraction patterns, which show a meridional reflection at  $\sim 4.7$  Å and an equatorial reflection at  $\sim 6-11$  Å (Fig. 2)<sup>7-10</sup>.

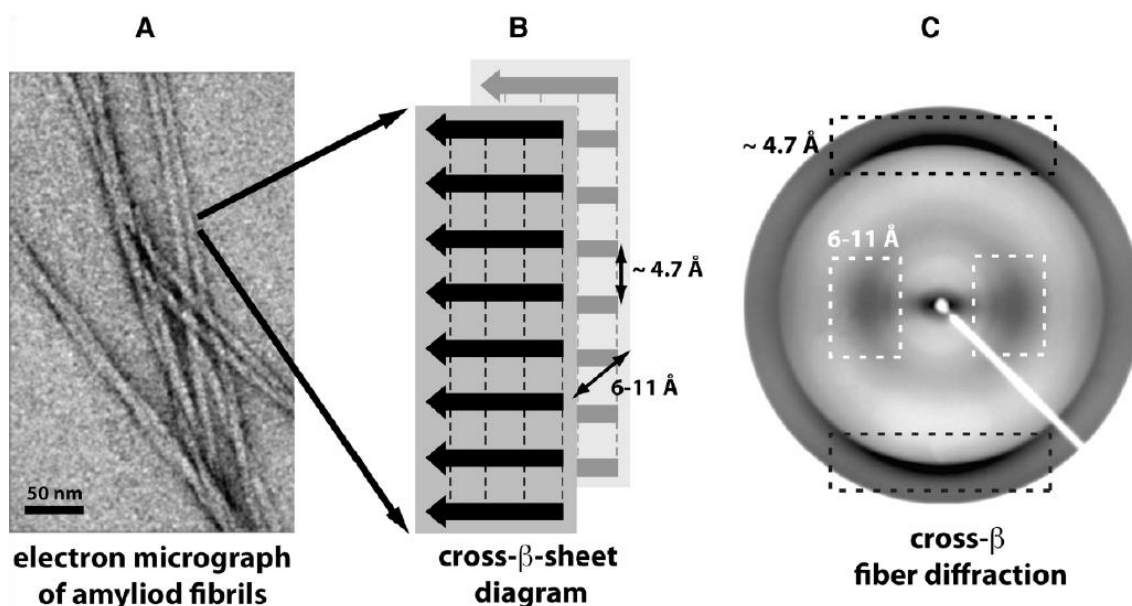


**Figure 2.** Underlying structure of Amyloids

(A) Amyloid fibrils are composed of long filaments that are visible in negatively stained transmission electron micrographs. (B) The schematic diagram of cross- $\beta$  sheets in a fibril, with the backbone hydrogen bonds represented by dashed lines, indicates the repetitive spacings that give rise to (C) the typical fiber diffraction pattern with a meridional reflection at  $\sim 4.7$  Å (black dashed box) and an equatorial reflection at  $\sim 6-11$  Å (white dashed box). This figure is reproduced from Greenwald, J. et al. 2010 with permission<sup>10</sup>.

There are many amyloid-forming proteins associated with more than 30 types of diseases, so-called amyloidosis including amyloid- $\beta$  ( $A\beta$ )<sup>11,12</sup> peptide with Alzheimer's disease, amylin<sup>13,14</sup> with diabetes type 2, and  $\beta_2$ -microglobulin ( $\beta_2m$ ) with dialysis-related amyloidosis (Table 1)<sup>6,7,15</sup>. However, many proteins not related to diseases has been found to form, under some conditions in vitro, amyloid fibrils<sup>7,16</sup>. This finding indicated that amyloid fibrillation is the generic ability of polypeptide chains and it has been further considered that most proteins have a potential to cause amyloidosis by amyloid deposition. Furthermore, amyloid fibrils are not only causative factors of diseases but also attract interests of researchers from the viewpoint of nanomaterials<sup>17</sup>. This is because functional amyloids present in insects, fungi and bacteria are important for maintaining the homeostasis of those organisms<sup>18</sup>. If controlling amyloid fibrillation could be accomplished, it may provide a novel therapeutic strategy for various diseases associated with amyloid fibrils.

Formation of amyloid fibrils can be divided into two main steps, nucleation and elongation phases (Fig. 3A)<sup>19-21</sup>. In the most cases, nucleation phase takes a considerably long time because of the high free-energy barrier existing between monomer protein and nucleus. Therefore, the duration of the nucleation phase is called the lag time when the formation of fibrils does not happen apparently. Once amyloid nuclei form, amyloid fibrillation occurs drastically. This phase is called elongation phase as the conversion rate of proteins into amyloid fibrils is the highest. In order to monitor the kinetics of amyloid fibrillation, there are several methods including light scattering, circular dichroism (CD) spectroscopy, infrared (IR) spectroscopy, fluorescence spectroscopy and so on. Among them, the fluorescence measurement with an amyloid specific fluorescence dye, thioflavin T (ThT)<sup>22</sup>, is the most widely used to assay amyloid fibrillation because it

provides a useful and convenient way to detect fibrillation in real-time. The birefringence of Congo Red-stained amyloid, appearing apple-green under polarized light, has been also used to detect fibrils with microscopy<sup>23</sup>.

**Table 1.** Some human diseases associated with amyloid aggregation

This table is produced from Knowles, T. P. J. et al. 2014<sup>15</sup>.

<b>Disease</b>	<b>Aggregating protein or peptide</b>	<b>Structure of protein or peptide</b>
<b><i>Neurodegenerative diseases</i></b>		
Alzheimer's disease	Amyloid- $\beta$ peptide	Intrinsically disordered
Parkinson's disease	$\alpha$ -synuclein	Intrinsically disordered
Amyotrophic lateral sclerosis	Superoxide dismutase 1	$\beta$ -sheet and Ig-like
Spongiform encephalopathies	Prion protein or its fragments	Intrinsically disordered and $\alpha$ -helical
Huntington's disease	Huntingtin fragments	Mostly Intrinsically disordered
<b><i>Non-neuropathic system amyloidosis</i></b>		
Amyloid light chain (AL) amyloidosis	Ig light chains or its fragments	$\beta$ -sheet and Ig-like
Amyloid A (AA) amyloidosis	Serum amyloid A1 protein fragments	$\alpha$ -helical and unknown fold
Haemodialysis-related amyloidosis	$\beta_2$ -microglobulin	$\beta$ -sheet and Ig-like
Lysozyme amyloidosis	Lysozyme mutants	$\alpha$ -helical and $\beta$ -sheet
<b><i>Non-neuropathic localized amyloidosis</i></b>		
Apolipoprotein A1 (Apo A-1) amyloidosis	Apo A-1 fragments	Intrinsically disordered
Diabetes type 2	Amylin	Intrinsically disordered
Injection-localized amyloidosis	Insulin	$\alpha$ -helical

On the other hand, amorphous aggregates have no ordered structure in contrast to amyloid fibrils. We often observe the precipitation of recombinant proteins as inclusion body during their expression. Similar to amyloid fibrils, this type of aggregate is also associated with various diseases represented by cataract<sup>24,25</sup>. However, there is no many researches focused on amorphous aggregates because amyloid fibrils are more attractive for researchers. Therefore, it is necessary to understand the amorphous aggregation phenomena for developing therapeutic strategies of several diseases and for advancing protein science.

In general, it is considered that the process of amorphous aggregation is faster than that of amyloid fibrillation, because nucleation is not required (Fig. 3B)<sup>26</sup>. Indeed, we can often observe rapid kinetics of amorphous aggregation depending on various conditions in vitro (e.g. salt, temperature, pH). This is because protein losses its native structure under denaturing conditions. Then, this conformational alteration lead to the exposure of hydrophobic groups of proteins that are buried in the nature structures<sup>27</sup>. These exposed hydrophobic groups may induce new intermolecular interactions resulting in amorphous aggregation<sup>28</sup>.

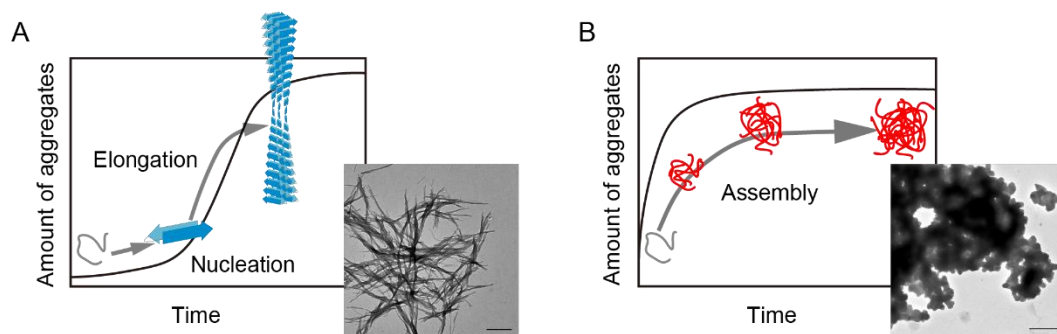


**Figure 3.** Difference of aggregation kinetics between (A) amyloid fibrils and (B) amorphous aggregates. Distinct morphologies are also shown by TEM observation. Scale bars on TEM images indicate 500 nm.

As mentioned above, it is obvious that there are two types of protein aggregates. However, the relationship between amyloid fibrils and amorphous aggregates focused on the formation pathways has not been understood in detail. The reason of this is the complexity of aggregation pathways. So far, studies examined either amyloid fibrils or amorphous aggregates. In this study, I focused on both of these aggregates simultaneously to obtain the comprehensive understanding of protein aggregation.

### **1.3 $\beta_2$ -microglobulin ( $\beta_2m$ )**

$\beta_2$ -microglobulin ( $\beta_2m$ ) is the light chain of the major histocompatibility complex class I (MHC I) and is expressed on almost all human nucleated cell surfaces and is normally present in most biological fluids including serum. It contains 99 amino acids with a molecular weight of 11,600. Their sequence has a high homology with the whole family of immunoglobulin molecules and  $\beta_2m$  forms a typical immunoglobulin domain fold, where two  $\beta$ -sheets are linked by a disulfide bond (Cys25-Cys80) and hydrophobic residues between them (Fig. 4)<sup>29-31</sup>.

It is known that dialysis-related amyloidosis (DRA) is caused by accumulation of amyloid fibrils of  $\beta_2m$  in the synovial membrane of carpal tunnel by long-term various dialysis including hemodialysis, hemofiltration and peritoneal dialysis<sup>32,33</sup>. Although the serum concentration levels of  $\beta_2m$  is maintained very low by being catabolized in renal tubules in healthy persons, accumulation of the proteins occur with the progress of renal failure. Therefore, in patients undergoing hemodialysis, the serum concentration of  $\beta_2m$  is significantly higher than those in healthy persons<sup>34</sup>. Thus, it is believed that this condition leads to amyloid fibrillation because protein aggregation is greatly affected by their concentration.

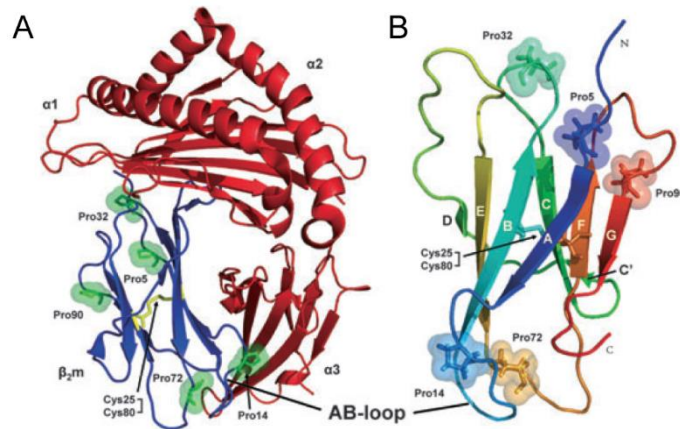


**Figure 4.** Structure of monomeric  $\beta$ 2m. (A) Cartoon representation of human MHC I (PDB code 3MYJ) and (B) monomeric native wild-type  $\beta$ 2m (PDB code 2XKS). This figure is reproduced from Eichner, T. & Radford, S. E. 2011 with permission<sup>35</sup>.

In *in vitro*, amyloid fibrillation of  $\beta$ 2m is greatly dependent on the pH of solvent. Although  $\beta$ 2m forms no amyloid fibrils under physiological conditions, it readily forms amyloid fibrils at low pH around 2.0-3.0<sup>36,37</sup>. At pH 2.5,  $\beta$ 2m loses the secondary and tertiary structures observed at pH 7.5<sup>38</sup>. Therefore, it is expected that unfolding or denaturation of native proteins is required to its assembly into amyloid fibrils<sup>39</sup>. Although  $\beta$ 2m easily forms the amyloid fibrils under low pH conditions with various agitation (e.g. shaking<sup>40</sup>, stirring<sup>41</sup>, ultrasonication<sup>42-44</sup>, laser irradiation<sup>45</sup> and so on), it is difficult to form amyloid fibrils without agitation even under low pH. Furthermore, salt concentration also plays one of important roles in amyloid fibrillation. Raman et al. demonstrated that cosolute anion interaction could modulate amyloid fibrillation by investigating the effects of various salts<sup>46</sup>. However, high concentrations of salts induced the amorphous aggregates. As described above, it was difficult to form amyloid fibrils under neutral pH. However, it has been found that  $\beta$ 2m forms amyloid fibrils in the presence of SDS<sup>47,48</sup> or TFE<sup>49,50</sup> under neutral pH.

Taken together,  $\beta$ 2m will be greatly useful for investigating the relationship between amyloid fibrils and amorphous aggregates, because both types of aggregates can form depending on conditions. Therefore, in this study, I used  $\beta$ 2m as a model protein of amyloid fibrillation and amorphous aggregation, and aim to construct the general mechanism of protein aggregation.

#### **1.4 Outline of this dissertation**

Although there are a large number of studies that investigate the protein aggregation, the principles of aggregation are not clear. Various models and mechanisms of protein aggregation have also been reported. In this study, I focused on the two types of aggregates, i.e., amyloid fibrils and amorphous aggregates, to elucidate the mechanism of protein aggregation. In order to achieve this aim, I performed a series of experiments addressing the effects of various factors on protein aggregation.

In the chapter 2, I demonstrated the competitive protein aggregation by studying the salt-concentration dependence and ultrasonic-intensity dependence. From these results, I could reveal that amyloid fibril formation and amorphous aggregation are supersaturation-limited and unlimited, respectively. These properties play the key role under the conditions where two types of aggregates form competitively.

In the chapter 3, the effects of temperature on protein aggregation were investigated to demonstrate the generality of competitive mechanism that described in chapter 2. In general, it has been considered that proteins form the aggregates at the high temperature. However, in this study, I observed the dissolution of protein aggregates and the unfolded state appeared at high temperature. Furthermore, this heat-induced dissolution of protein aggregates could be explained by adopting the competitive protein aggregation mechanism.

Both in the chapters 2 and 3, I tried to address the mechanism of protein aggregation on the basis of conformational phase diagram. Consequently, I could obtain the phase diagram dependent on respective effects (salt-concentration, ultrasonic-intensity and temperature). Taken together, I propose that competitive formations of amyloid fibrils and amorphous aggregates under various conditions can be understood comprehensively.

Chapter 2. Supersaturation-limited and unlimited phase transitions compete to produce the pathway complexity in amyloid fibrillation

## 2.1 Introduction

The aggregates of denatured proteins were classified into two types; amyloid fibrils and amorphous aggregates. Amyloid fibrils are fibrillar aggregates with a width of approximately 10 nm and length of several micrometers<sup>7,8,51,52</sup>. The dominant secondary structure is a cross- $\beta$  structure stabilized by an ordered hydrogen bond network. Although they were found to be associated with more than 30 types of amyloidosis including dialysis-related amyloidosis caused by  $\beta$ 2m, various proteins not associated with diseases have also been shown to form amyloid fibrils, indicating that amyloid fibrillation is a generic property of denatured proteins<sup>7</sup>. Previous studies proposed that amyloid fibrils formed in the supersaturated solutions of precursor proteins through a nucleation and growth mechanism that was characterized by a lag phase or via seed-dependent growth without a lag phase<sup>19,21,53</sup>. We revisited "supersaturation" and argued its critical involvement in amyloid fibrillation<sup>43,54-57</sup>. It is noted that the role of supersaturation in the kinetics and thermodynamics of fiber formation of hemoglobin S, which is associated with sickle cell anemia, has been studied extensively<sup>58,59</sup>. The role of supersaturation at the proteome level in neurodegenerative diseases has recently been reported<sup>60</sup>.

On the other hand, the term amorphous aggregate has been collectively used for other types of aggregates<sup>61</sup>, which have not been targets of intensive research. We previously suggested that amyloid fibrils and amorphous aggregates were similar to the crystals and glasses of substances, respectively<sup>43</sup>, and that they are represented by the same phase diagram as often used for crystallization of substances (Fig. 1A). Nevertheless, the relationship between amyloid fibrils, amorphous aggregates, and related aggregates such as oligomers or curvilinear fibrils has not yet been elucidated in detail<sup>61,62</sup>. One of the most important issues for clarifying the mechanism of protein aggregation is whether

amorphous aggregates including oligomers or protofibrils represent on-pathway intermediates leading to amyloid fibrils or off-pathway dead products (Fig. 1B).

Various kinds of agitations such as shaking<sup>40</sup>, stirring<sup>41</sup>, or ultrasonic irradiation<sup>42-44,63,64</sup> have been shown to effectively force spontaneous fibrillation under conditions in which no fibrillation was expected because of the persistent metastability of supersaturation. In the case of ultrasonication-forced fibrillation, I suggested that interactions with hydrophobic surfaces of cavitation bubbles condensed proteins, leading to the breakdown of supersaturation and then fibrillation<sup>43,64</sup>. Ultrasonication is now recognized as one of the important approaches for elucidating the mechanisms underlying amyloid fibrillation<sup>64-66</sup>.

When we monitored the ultrasonication-dependent fibrillation of proteins thioflavin T (ThT), we often observed a significant decrease in ThT fluorescence after the burst-phase increase<sup>44,66-68</sup>. The decrease in ThT fluorescence was accelerated when the lag time was shorter, suggesting that this reduction was caused by the ultrasonication-dependent transformation of preformed fibrils into distinct conformational states<sup>44,66,67</sup>. Combined with the salt concentration-dependent competition between fibrillation and amorphous aggregation, I showed that a competitive mechanism, in which various amyloidogenic and non-amyloidogenic aggregates competed (Fig. 1B, Model 2), explained comprehensively the kinetics and thermodynamics of protein aggregation.

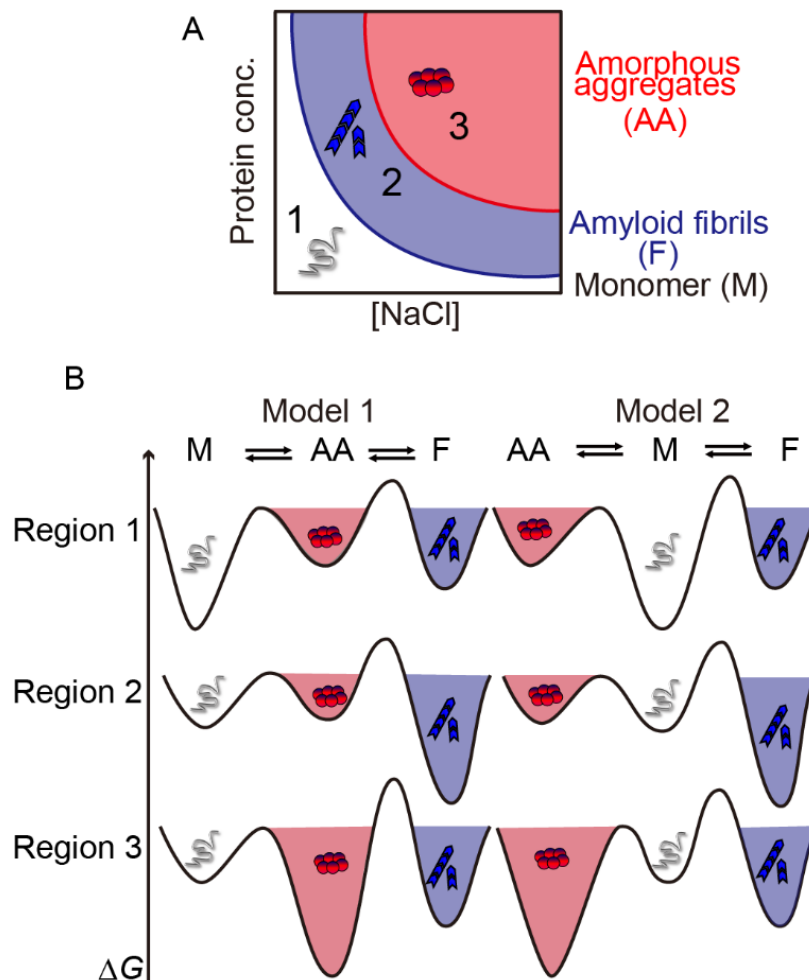


**Figure 1.** General phase diagram for the conformational transitions of proteins. (A) Salt- and protein concentration-dependent conformational phase diagram of  $\beta 2m$  under acidic conditions is illustrated. The regions of unfolded monomers (Region 1), amyloid fibrils (Region 2), and amorphous aggregates (Region 3) are shown. (B) Relative free energies of monomers (M), amorphous aggregates (AA) and amyloid fibrils (F) under distinct regions of phase diagram are compared between a consecutive model (Model 1) with on-pathway AA and competitive model (Model 2) with off-pathway AA. Free energy barriers between the conformational states are also included assuming that the barriers for amyloid fibrils are higher than those for amorphous aggregates. This figure is reproduced from Adachi, M. et al. 2015 with permission<sup>69</sup>.

## 2.2 Materials and methods

### *Proteins and chemicals*

A recombinant human  $\beta$ 2m protein with an additional methionine residue at the N terminus was expressed in *Escherichia coli* and purified as previously reported<sup>70</sup>. ThT was obtained from Wako Pure Chemical Industries, Ltd. (Osaka, Japan). All other reagents were purchased from Nacalai Tesque (Kyoto, Japan).

### *Amyloid fibrillation under ultrasonication*

Lyophilized  $\beta$ 2m was dissolved in 10 mM HCl. The concentration of  $\beta$ 2m was determined spectrophotometrically using a molar extinction coefficient of  $19,300 \text{ M}^{-1} \text{ cm}^{-1}$  at 280 nm based on its amino acid composition. The sample solution of 1 mL in a disposable cuvette with a 1-cm light path contained 25  $\mu\text{M}$   $\beta$ 2m, 0.1 M NaCl, 5  $\mu\text{M}$  ThT, and 10 mM HCl. I used a water bath-type ultrasonic transmitter with a temperature controller (ELESTEIN, Elekon Science Co., Chiba, Japan) to induce fibrillation<sup>44,63</sup>. A cycle involving 1 min of ultrasonication and 9 min of quiescence was repeated. The temperature of the water bath was set to 37 °C.

I measured temperature increases due to ultrasonication with a thermocouple (Compact Thermologger AM-8000K, Anritsu, Tokyo, Japan) to monitor the strength of ultrasonication. Among the several methods employed to determine ultrasonic power, calorimetry is often used to specify the ultrasonic power dissipated into a solution, in which the initial rate of the temperature increase is measured upon irradiation of the solution with ultrasonic pulses<sup>65</sup>. With the calorimetric method, ultrasonic power ( $Q$ ) was calculated using the equation:  $Q = (dT/dt) C_p M$ , where  $C_p$  is the heat capacity of water ( $4.2 \text{ J g}^{-1} \text{ K}^{-1}$ ),  $M$  is the mass of water (g), and  $(dT/dt)$  is the increase in temperature per second. In other words, with the same sample volumes,  $(dT/dt)$  was proportional to

ultrasonic power.

Amyloid fibrillation was detected by ThT fluorescence with an excitation wavelength of 445 nm and emission wavelength of 485 nm using the Hitachi fluorescence spectrophotometer F7000 or F4500 (Tokyo, Japan). ANS fluorescence was also monitored with the same fluorometers with an excitation wavelength of 350 nm and emission wavelength of 485 nm.

The seeding experiments were performed by adding 5% (v/v) seeds to the monomeric  $\beta$ 2m solution. Seed fibrils were prepared by ultrasonication as described above. Kinetics were monitored using a SH9000 microplate reader (Corona Electric. Co., Ibaraki, Japan).

#### *Amyloid fibrillation in the presence of NaCl*

The sample solution of 2 mL in a glass cuvette with a 1-cm light path contained 25  $\mu$ M  $\beta$ 2m, 5  $\mu$ M ThT, 50  $\mu$ M ANS, 10 mM HCl, and various concentrations of NaCl. ThT and ANS fluorescence under stirring with a stirring bar was measured with the F7000 fluorescence spectrometer. Excitation and emission wavelengths were the same as those described above.

#### *Circular dichroism (CD), atomic force microscopy (AFM) and transmission electron microscopy (TEM)*

Far-UV CD spectra were measured with a Jasco J720 spectropolarimeter (Tokyo, Japan) as described previously<sup>63</sup>. Measurements were performed at 25 °C using a quartz cuvette with a 1 mm path length, and the results were expressed as mean residue ellipticity  $[\theta]$ .

AFM images were obtained using a Digital Instruments Nanoscope IIIa scanning microscope (Veeco Instruments Inc., Plainview, NY) as described previously<sup>66</sup>.

Regarding TEM measurements, 10-fold diluted samples were spotted onto a collodion-coated copper grid (Nisshin EM Co., Tokyo, Japan). After 1 min, the remaining solution was removed with filter paper and 5  $\mu$ L 2% (w/w) ammonium molybdate was spotted. After 1 min, the remaining solution was removed in the same manner. TEM (Hitachi H-7650, Tokyo, Japan) images were obtained at 20 °C with a voltage of 80 kV and magnification of 20,000.

#### *Fourier transform infrared spectroscopy (FTIR)*

FTIR measurements were carried out on a Bruker Equinox 55 (Bruker, Germany) instrument equipped with an MCT detector in CaF<sub>2</sub> cells with 100  $\mu$ m teflon spacers at 1 cm<sup>-1</sup> resolution as described previously<sup>56</sup>. To avoid the contribution of water vapor peaks to the spectra, the instrument was purged with dry-air. Native and acid unfolded monomeric  $\beta$ 2m solutions were prepared by dissolving the lyophilized  $\beta$ 2m powder in D<sub>2</sub>O solutions containing 10 mM Na-phosphate, 0.1 M NaCl, pD 7.5 or ~10 mM DCl, 0.1 M NaCl, respectively.

Amyloid fibrils were induced in a disposable cuvette with a 1-cm light path by stirring or with the same cycles of ultrasonication and quiescence. Then, fibrillar samples were concentrated by centrifugation for 30 min at 40,000 rpm with a Beckman TL-100 ultracentrifuge using a TLA100.3 rotor. The supernatant was used as a background reference.

The spectra shown were baseline subtracted, corrected for vapor and HDO contamination and normalized to an area that is approximately equal to that of a 5 mg/mL protein solution. The second derivative of the spectra were used to determine the positions of the components<sup>71</sup>. The fitting was performed by fitting Gaussian functions to the original curve. The width of the Gaussian curves were limited to <20 cm<sup>-1</sup>. Components

at 1585, 1600 and 1612  $\text{cm}^{-1}$  and above 1700  $\text{cm}^{-1}$  are considered as side chain signals.

The secondary structure content (%) was calculated from the area of the fitted components.

## 2.3 Results

### *Ultrasonication-forced amyloid fibrillation*

I examined the dependence of  $\beta$ 2m fibrillation on ultrasonic power by using different positions of the ultrasonicator bath. Amyloid fibrillation was monitored by ThT fluorescence at 485 nm (Fig. 2A). I simultaneously monitored ultrasonic power by measuring temperature increases in the sample solution (Fig. 2B). With cycles of 1 min of ultrasonication and 9 min of quiescence, the marked increase observed in temperature during ultrasonic irradiation was followed by a slightly slower decrease in temperature, and a constant temperature was maintained for 5 min. I assumed that the maximal increase in temperature was approximately proportional to  $(dT/dt)$  and, thus, ultrasonic power.

Distinct kinetics were observed depending on ultrasonic power (Fig. 2A-C). When ultrasonic power was weak, as represented by a small increase in temperature (i.e., 4 °C), the amyloid burst occurred after a lag time of 4 h. With increasing ultrasonic power (i.e., a temperature increase of 7 °C), the lag time was shortened to 2 h and accompanied by a decrease in the maximal ThT fluorescence. A gradual decrease in ThT fluorescence was then observed (Fig. 2A). When fibrillation was monitored under strong ultrasonic power (i.e., a temperature increase of 17 °C), the lag time was further shortened to 1 h and accompanied by only a small increase in ThT fluorescence followed by a subsequent decrease. These ultrasonic power-dependent decreases in the lag time and ThT fluorescence (Fig. 2C) were consistent with our previous studies on  $\beta$ 2m<sup>44,66</sup> and findings on  $\alpha$ -synuclein fibrils<sup>68</sup> and A $\beta$ (1-40) fibrils<sup>67</sup>, implying that extensive ultrasonication transformed the preformed fibrils to amorphous aggregates. In addition, the decrease observed in maximal ThT fluorescence with an increase in ultrasonic power suggested the direct formation of amorphous aggregates as well as amyloid fibrils. However, this

was not the case for  $\beta$ 2m, as will be described later.

Here, to check the effects of an increase in temperature on fibrillation, spontaneous fibrillation of 25  $\mu$ M  $\beta$ 2m in 0.1 M NaCl, 5  $\mu$ M ThT, and 10 mM HCl was monitored in the presence or absence of stirring at several temperatures using the Hitachi fluorescence spectrophotometer F4500 (Fig. 2D). The stirring accelerated the fibrillation and higher temperature slightly increased the rate of fibrillation. However, without stirring, no fibrillation occurred even after 6 hr at any temperatures. The intrinsic decrease in ThT fluorescence upon increasing the temperature caused the decrease in the final ThT fluorescence. In my ultrasonication experiments, the increase in temperature occurred only transiently (Fig. 2B) and the stirring effects caused by ultrasonic irradiation may not be significant. Thus, although ultrasonication is linked with the increase in temperature and the increase in temperature may be one of the important factors accelerating fibrillation, I do not consider that the increase in temperature is a major driving force of amyloid fibrillation and fibrillation is dominantly accelerated by ultrasonication-dependent cavitation.

#### *Morphologies and secondary structures of ultrasonication-induced products*

I analyzed the morphologies of ultrasonication-induced products by AFM and TEM. Under the condition of weak ultrasonic power, typical short fibrils were produced after the lag time and were further fragmented by extensive ultrasonication (Fig. 2G-I). Although similar morphological changes were observed under the condition of stronger ultrasonic power, amyloid particles were finer than those under weaker ultrasonic power (Fig. 2J, K). The formation of amorphous aggregates was unclear; however, I sometimes observed clumps, suggesting amorphous aggregates. I examined the secondary structures by measuring far UV CD spectra (Fig. 2E, F).  $\beta$ 2m monomers were largely disordered at

pH 2.0 in 10 mM HCl and 0.1 M NaCl. After the ThT burst induced by the ultrasonic irradiation of weak power, transformation to the spectrum of a typical  $\beta$ -sheet structure was observed (Fig. 2F). Similar changes in the spectrum were observed even under the conditions of strong ultrasonic power, in which only a slight increase in ThT fluorescence was noted (Fig. 2E). These results suggested that, in the case of  $\beta$ 2m, strong ultrasonic power induced "amyloid-like"  $\beta$  structures, without strong ThT fluorescence. Although further ultrasonication decreased ThT fluorescence, the CD spectrum of the  $\beta$ -sheet structure remained, indicating that extensive ultrasonic irradiation to the preformed fibrils did not destroy the  $\beta$ -sheet structure. These results were distinct from those for  $\alpha$ -synuclein<sup>68</sup> or A $\beta$ (1-40)<sup>67</sup>, in which strong ultrasonic irradiation to the preformed fibrils changed the CD spectra from those of  $\beta$ -structures to those of highly disordered structures.

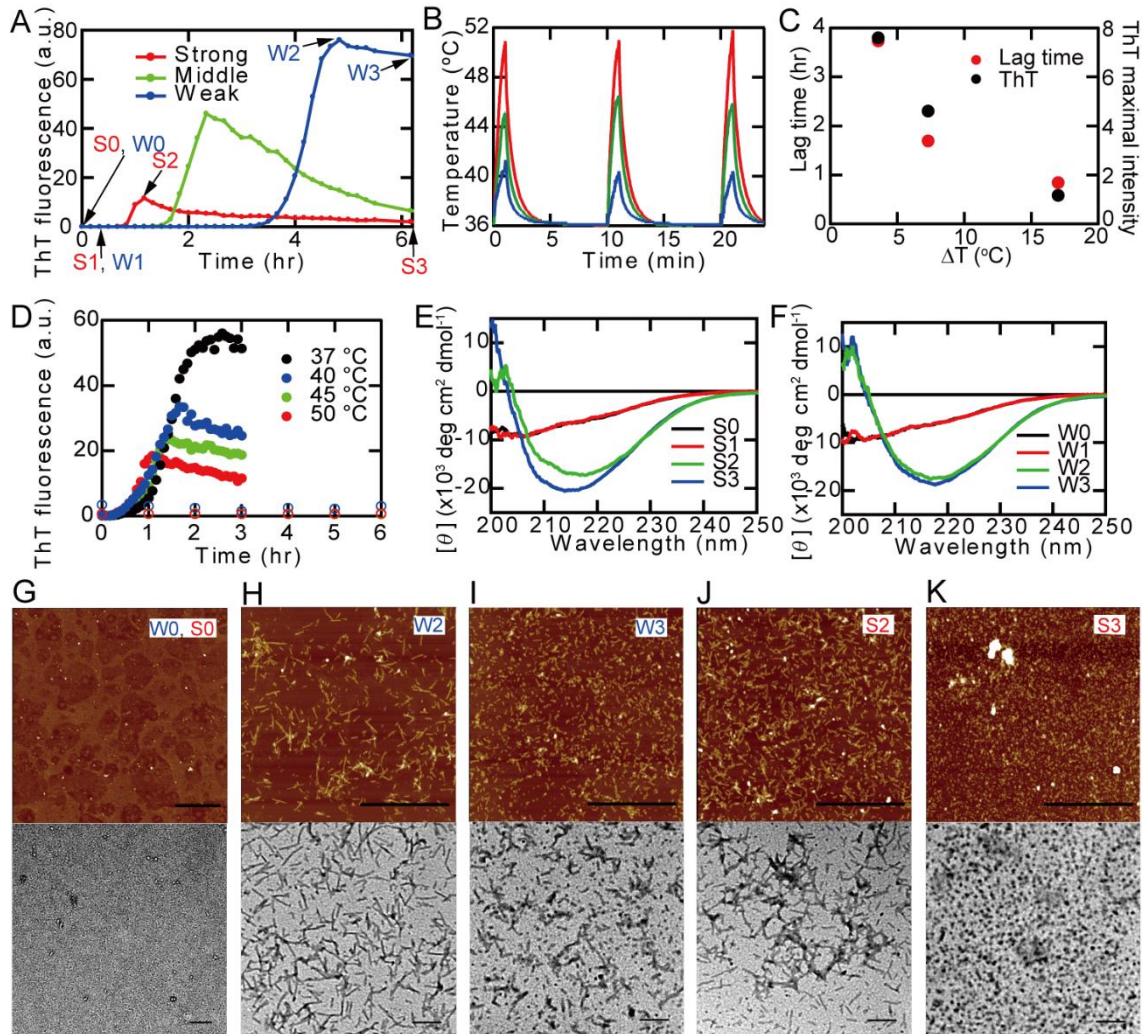


**Figure 2.** Ultrasonication-forced amyloid fibrillation of  $\beta$ 2m under various levels of ultrasonic power. (A) Fibrillation kinetics of 25  $\mu$ M  $\beta$ 2m at 10 mM HCl, 0.1 M NaCl and 5  $\mu$ M ThT monitored by ThT fluorescence at 485 nm. (B) Change in temperature during cycles of 1 min of ultrasonication and 9 min of quiescence under various levels of ultrasonic power as monitored by a thermocouple. The temperature of the water bath was set to 37 °C. (C) The dependence of the lag time on temperature increases. (D) Fibrillation kinetics at various temperatures in the presence (solid symbols) or absence (open symbols) of stirring directly monitored using the fluorescence spectrophotometer. Fluorescence intensities in A and D cannot be compared because of the difference in settings. (E, F) CD spectra of samples under strong (E) and weak (F) ultrasonic power. (G-K) AFM and TEM images of aggregates formed under weak (G-I) and strong (J, K) ultrasonic power. The time points for preparation of samples shown in panels (E-K) were indicated in (A). The scale bars on the AFM and TEM images indicate 1  $\mu$ m and 200 nm, respectively. This figure is reproduced from Adachi, M. et al. 2015 with permission<sup>69</sup>.

I then used FTIR to examine the secondary structures of fibrillar aggregates as well as other conformational states (Table 1 and Fig. 3). The advantages of FTIR spectroscopy are that  $\beta$ -sheet structures can be distinguished from other structures more clearly than by CD<sup>71,72</sup> and that antiparallel  $\beta$ -structures can also be identified, depending on the presence of a small but sharp high frequency peak at 1690-1695  $\text{cm}^{-1}$  in non-deuterated and at 1682-1685  $\text{cm}^{-1}$  in deuterated form<sup>71</sup>.

Native  $\beta$ 2m showed  $\beta$  components around 1636 and 1690  $\text{cm}^{-1}$  which are related to antiparallel  $\beta$  structures. In contrast, acid denatured  $\beta$ 2m was proven to be largely disordered. In most of the fibril samples, I observed the dominant intermolecular  $\beta$  components appearing at 1620-1622  $\text{cm}^{-1}$  accompanied by minor, native-like  $\beta$  components around 1632-1636  $\text{cm}^{-1}$ . The intermolecular  $\beta$  components may represent parallel  $\beta$  structures considering the absence of a clear high frequency peak. I have to note that the fibrils formed under strong sonication and, at a lower level, the mature fibrils experienced strong sonication, tended to contain visible large aggregates. Their spectral amplitudes were lower and the spectra were noisier, probably because of inhomogeneity of the samples.

Taken together, the FTIR spectra of ultrasonicated fibrils were consistent with the CD spectra indicating that, although the strong ultrasonic irradiation did not produce fibrils with marked ThT fluorescence, fibrils with secondary structures similar to those of mature amyloid fibrils were formed.

**Table 1.** Secondary structure assignments of various conformational states of  $\beta 2m$  on the basis of FTIR spectra. Experiments were carried out in  $D_2O$  solutions and pD is the pH meter reading in  $D_2O$ . This table is reproduced from Adachi, M. et al. 2015 with permission<sup>69</sup>.

Conformation (conditions)	Major components	Wave number $cm^{-1}$	Fraction %	Structure assignment
Native (pD 7.5)	Antiparallel $\beta$ -sheet	1636	48	$\beta$
		1646	18	Random
		1659	15	Turn
		1673	18	Turn
		1690	1.4	High frequency antiparallel $\beta$
Acid denatured (pD 2.0, 0.1 M NaCl)	Disordered	1632	1	$\beta$
		1640	68	Random
		1668	31	Turn
		1693	0.1	High frequency antiparallel $\beta$
		1620	41	$\beta$
Fibrils formed by stirring (pD 2.0, 0.1 M NaCl)	Parallel $\beta$ -sheet	1634	10	$\beta$
		1644	22	Random
		1661	21	Turn
		1683	5	Turn/high frequency Antiparallel $\beta$
		1616	19	$\beta$
Amorphous aggregates (pD 2.0, 1.0 M NaCl)	Antiparallel $\beta$ -sheet	1634	40	$\beta$
		1650	6	Random/helix
		1664	31	Turn
		1685	3	High frequency antiparallel $\beta$
		1621	34	$\beta$
Fibrils formed under strong sonication (pD 2.0, 0.1 M NaCl)	Parallel $\beta$ -sheet	1636	14	$\beta$
		1649	19	Random
		1664	19	Turn
		1681	14	Turn/high frequency antiparallel $\beta$ ?
		1620	27	$\beta$
Fibrils formed under weak sonication (pD 2.0, 0.1 M NaCl)	Parallel $\beta$ -sheet	1632	37	$\beta$
		1649	14	Random
		1662	18	Turn
		1682	3	Turn/high frequency Antiparallel $\beta$ ?
		1622	38	$\beta$
Strongly sonicated fibrils after formation by weak sonication (pD 2.0, 0.1 M NaCl)	Parallel $\beta$ -sheet	1635	15	$\beta$
		1648	24	Random
		1664	18	Turn
		1685	5	Turn/high frequency antiparallel $\beta$ ?
		1622	38	$\beta$

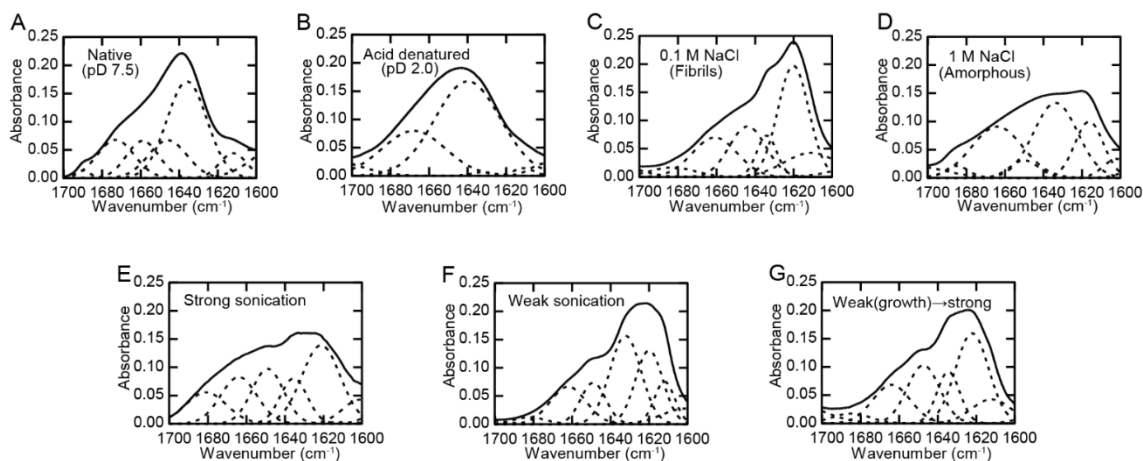


**Figure 3** FTIR spectra of various conformational states of  $\beta 2m$  in 10 mM DCl and  $D_2O$ . (A) The native state of  $\beta 2m$  at, as exception, pD 7.5 in 10 mM Na-phosphate, 0.1 M NaCl. (B) The acid-denatured monomer state. (C) Amyloid fibrils formed in 0.1 M NaCl. (D) Amorphous aggregates in 1.0 M NaCl. (E, F) Fibril samples prepared under strong (E)

and weak (F) ultrasonic power, respectively. (G) Extensively ultrasonicated fibrils after fibrillation under weak ultrasonic power. The solid lines represent the raw data and broken lines represent the deconvoluted spectra. The fitted spectra (not shown) on the basis of deconvoluted spectra were practically the same as the raw data. This figure is reproduced from Adachi, M. et al. 2015 with permission<sup>69</sup>.

#### *ANS binding and size distribution of ultrasonication-induced products*

ANS is an amphiphilic fluorescence dye that specifically interacts with the water-accessible hydrophobic surface of proteins<sup>68,73</sup>. I examined the interaction of ANS with amyloid fibrils and their products formed by extensive ultrasonication with different levels of ultrasonic power (Fig. 4B). Under both strong and weak ultrasonic power, ANS fluorescence increased with the formation of amyloid fibrils and decreased with further ultrasonic irradiation. The rate of the decrease was accelerated under the stronger ultrasonic power. The kinetics of the increase and decrease in ANS fluorescence were similar to those of ThT fluorescence, suggesting that the change in the binding regions for ThT and ANS occurred simultaneously.

Considering the possibility that decreases in ANS or ThT fluorescence occurred by the chemical decomposition of the dyes, I added ANS or ThT to samples with decreased fluorescence intensities (Fig. 4A, B). However, no increase was observed in ANS or ThT fluorescence, confirming that the decreases in ANS or ThT fluorescence were not caused by the decomposition of dyes. These results suggested that extensive ultrasonication decreased the ANS-specific exposed hydrophobic surfaces of fibrils, as well as the amyloid-specific surfaces detected by ThT.

I investigated the size distribution of the extensively ultrasonicated products by analytical ultracentrifugation (Fig. 4C, D). The distribution of sedimentation coefficient

(s) was estimated from the boundary curves of sedimentation velocity using sedfit software. As for the products under strong ultrasonic power,  $s$  values were distributed with two maxima at 18 and 27 s (Fig. 4E). On the other hand, regarding the products under weak ultrasonic power,  $s$  values were distributed with a broad maximum at 43 s (Fig. 4F). Thus, the sizes of aggregates appeared to be larger under the weaker ultrasonic power, which is consistent with the AFM or TEM measurements (Fig. 2). The strongly-sonicated fibrils with components of 18 and 27 s were considered to have solubility of the former higher than the latter and higher than that of fibrils grown under weak-sonication.

To further explore the effects of the extensive ultrasonication of preformed fibrils, I performed seeding experiments using fibrils at various stages of decreases in ThT fluorescence (Fig. 4G, H). When seed fibrils with almost no ThT fluorescence were used, the final ThT intensity was approximately 50% of the control fibrils, although the reaction was accelerated. These faster reactions were caused by the ultrasonication-induced fragmentation of fibrils. On the other hand, the decrease observed in the ThT intensity suggested that the seed fibrils trapped the monomers to prevent further fibrillation. Thus, extensively ultrasonicated fibrils may reduce the potential of efficient seeds.

I also examined the effects of extensive ultrasonication on the chemical structures of  $\beta$ 2m (Fig. 4I, J). An analysis with the reverse-phased HPLC showed that  $\beta$ 2m monomers depolymerized from fibrils with decreased ThT fluorescence by 4 M guanidine HCl had the same retention time as that of the control monomers. An analysis with mass spectrometry confirmed the intactness of  $\beta$ 2m molecules depolymerized from fibrils. Thus, the marked decreases observed in ThT fluorescence were not caused by the chemical decomposition of  $\beta$ 2m molecules.

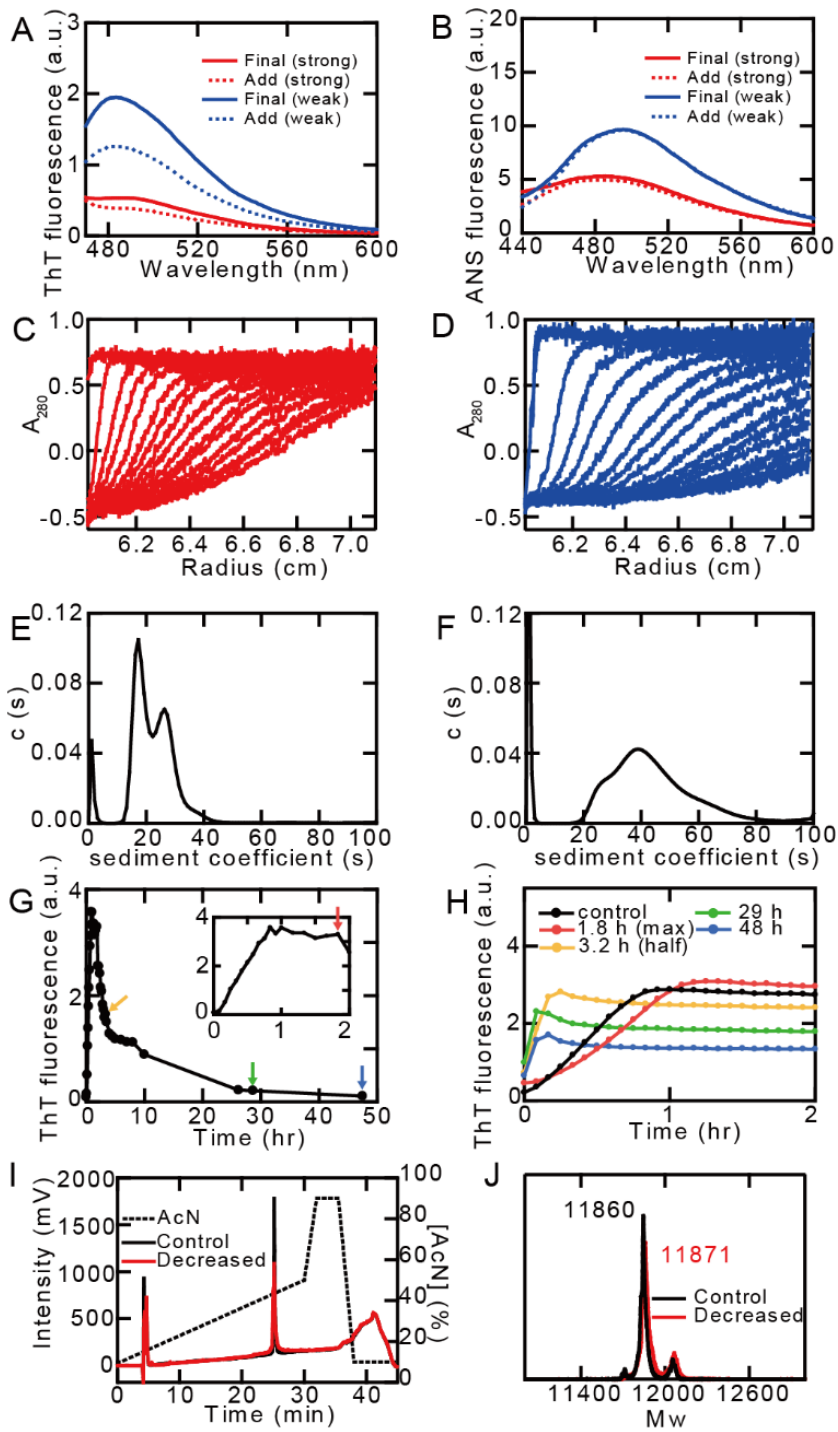


**Figure 4.** Analysis of ultrasonication-induced products. (A, B) Fluorescence spectra to monitor the effects of additional ThT (A) or ANS (B) on samples of reduced fluorescence intensities under strong and weak ultrasonic power. (C, D) Boundary curves of sedimentation velocity for products under strong (C) and weak (D) ultrasonic power. (E, F) Sedimentation coefficient distributions derived from sedimentation boundary profiles under strong (E) and weak (F) ultrasonic power. (G) Ultrasonication-forced fibrillation to prepare seed fibrils monitored by ThT fluorescence at 485 nm. The inset indicates expanded kinetics within 2 h. The sample solution contained 25  $\mu$ M  $\beta$ 2m, 0.1 M NaCl, 5  $\mu$ M ThT, and 10 mM HCl. (H) Seeding reactions with seed fibrils (5% (v/v)) obtained at various stages of fibrillation, as shown in (G). (I, J) Effects of extensive ultrasonication on chemical structures of  $\beta$ 2m. Extensively ultrasonicated fibrils with decreased ThT fluorescence were analyzed by reverse-phased HPLC (I) and mass spectrometry (J) after depolymerization by 4 M Gdn-HCl. This figure is reproduced from Adachi, M. et al. 2015 with permission<sup>69</sup>.

### *Salt-dependent fibrillation and aggregation*

Our laboratory previously showed that, although fibrillation was accelerated by low concentrations of NaCl of approximately 0.1 M, concentrations higher than 0.5 M inhibited fibrillation and induced amorphous aggregates<sup>43,46</sup>. To compare the products produced in the presence of high salt levels and extensive ultrasonication, I examined NaCl concentration-dependent competition between fibrillation and amorphous aggregation. Amyloid fibrillation in the presence of various concentrations of NaCl in 10 mM HCl was monitored by ThT and ANS fluorescence (Fig. 5A-H).

No significant change was observed in ThT in the absence of NaCl; however, a small increase in ANS fluorescence was noted within the dead time of the measurements (i.e., approximately 20 sec). Burst increases in ThT and ANS fluorescence were observed in the presence of 0.05 M NaCl after a lag time of 2.5 h. The marked increase in ANS fluorescence at 0.05 M was attributed to electrostatic attractions between negatively charged ANS and positively charged amyloid fibrils (see below). The lag time became shorter with increases in the concentration of NaCl. At 0.3 M NaCl, I clearly observed two-step kinetics monitored by ANS, whereas ThT fluorescence showed typical kinetics with a lag time of 0.5 h. At 0.4 M NaCl, ANS fluorescence showed fast and major saturating kinetics, followed by slow and small increases in ThT fluorescence. Only a very rapid increase in ANS fluorescence was observed at 1.0 M NaCl.

The end products at various concentrations of NaCl were examined by far-UV CD (Fig. 5I). In the absence of NaCl, the spectrum showed a largely disordered conformation. Typical  $\beta$ -structures were observed at 0.05 and 0.1 M NaCl. At NaCl concentrations higher than 0.2 M, the CD intensity decreased due to the precipitation of

aggregates. Yoshimura et al. reported that the main products at higher concentrations of NaCl were amorphous aggregates on the basis of AFM and TEM images<sup>43</sup>.

I also measured the FTIR spectrum of amorphous aggregates formed in 1.0 M NaCl (Fig. 3D). Interestingly, the spectrum showed an altered intermolecular  $\beta$  component around  $1616\text{ cm}^{-1}$  and an increased  $1634\text{ cm}^{-1}$  peak together with a small but sharp high frequency component, suggesting that the amorphous aggregates contain a large amount of antiparallel  $\beta$  components.

Previously, a similar secondary structure composition was observed for amorphous aggregates of  $\beta 2m$  formed at pD 5.5, close to the isoelectric point of the protein<sup>71</sup>. It is not rare that amorphous aggregates exhibit high  $\beta$ -sheet content. Among them, Bramanti et al.<sup>74</sup> reported  $\beta$ -structured amorphous aggregates of A $\beta$ (1-40) peptide induced by ferulic acid and Arosio et al.<sup>75</sup>, showed that non-amyloidogenic  $\lambda$  light-chain dimers form amorphous aggregates with increased  $\beta$ -sheet content. In addition, the disagreement between the CD and FTIR results suggests that the extensive precipitation of the aggregates in 1 M NaCl prevented the accurate secondary structure analysis by CD.

The plot of ThT fluorescence against NaCl concentrations showed a maximum at 0.2 M and decreased with a further increase in the NaCl concentration (Fig. 5J). Because the slower phase of the two-step increase in ANS fluorescence occurred at the same time range as the increase in ThT fluorescence, it represented the formation of fibrils (Fig. 5E). On the other hand, Yoshimura et al. showed that amorphous aggregates formed relatively rapidly without a lag phase<sup>43</sup>. Thus, I plotted intensity at 485 nm at 0.5 h, which may represent the amount of amorphous aggregates, and the final maximal value, which represents a sum of the amounts of amyloid fibrils and amorphous aggregates (Fig. 5J). ANS fluorescence at 0.5 h increased above 0.2 M NaCl and was saturated at 0.5 M NaCl.

The final ANS fluorescence peaked at 0.05 M NaCl and was constant above 0.1 M NaCl. The markedly strong ANS fluorescence at 0.05 M NaCl may have been caused by the electrostatic binding of negatively charged ANS molecules to positively charged  $\beta$ 2m fibrils.

Although I assume that oligomers and amorphous aggregates might be continuous as proposed by Miti et al.<sup>62</sup>, I cannot address the properties of oligomers at this stage because I did not observe oligomers in this study.

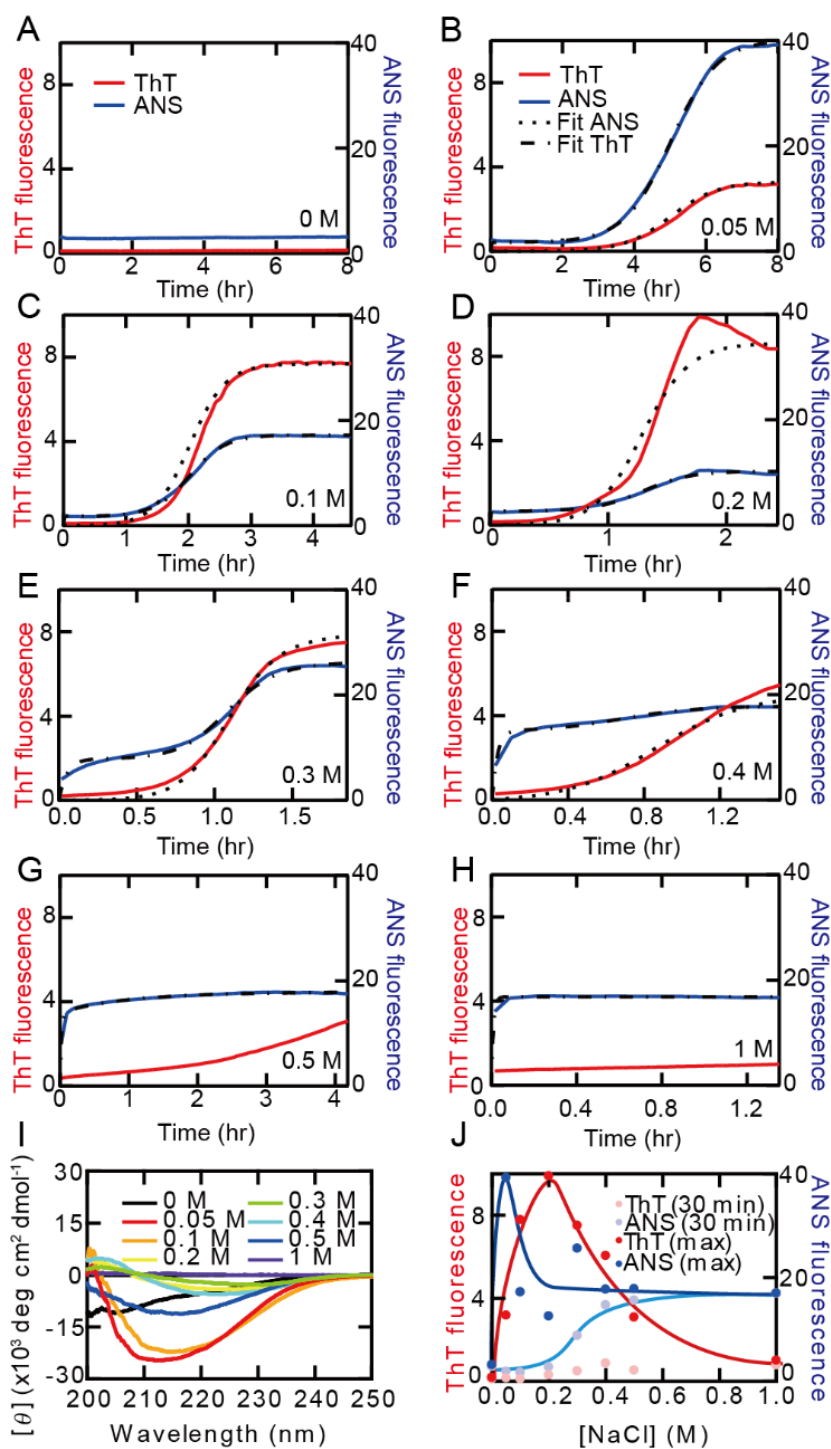


**Figure 5.** Dependence of amyloid fibrillation of  $\beta$ 2m on the NaCl concentration. The kinetics of protein aggregation in 10 mM HCl at 37 °C were measured by observing ThT fluorescence at 485 nm (red) and ANS (blue) fluorescence at 485 nm. NaCl concentrations were 0 (A), 0.05 (B), 0.1 (C), 0.2 (D), 0.3 (E), 0.4 (F), 0.5 (G), and 1.0 M (H). The broken lines are the fitted curves. (I) CD spectra after aggregation at various concentrations of NaCl. (J) Dependencies on the NaCl concentration of the ThT and ANS fluorescence values at 0.5 h and maximum. This figure is reproduced from Adachi, M. et al. 2015 with permission<sup>69</sup>.

## 2.4 Discussion

### *Competitive model of amyloid fibrillation and amorphous aggregation*

I proposed a competitive mechanism of amyloid fibrillation and amorphous aggregation to explain NaCl concentration-dependent changes in end products (Model 2 in Fig. 1B and Mechanism 1 in Fig. 6A)<sup>43,54,68</sup>. A similar competitive mechanism was reported previously for amyloidogenic light chains<sup>76,77</sup>,  $\beta$ 2m<sup>78</sup>, insulin<sup>79</sup>, and  $\alpha$ -synuclein<sup>80,81</sup>, in which the aggregation process was branched, with one pathway leading to fibrils and another to oligomeric intermediates that may ultimately form amorphous aggregates. Miti et al.<sup>62</sup> recently reported a similar mechanism with hen egg white lysozyme at pH 2 and 52 °C including various stable, metastable, and kinetically trapped amyloid aggregate phases. They focused on transitions from monomers to oligomers, curvilinear fibrils, and oligomeric precipitation, and proposed that oligomeric and amorphous aggregates were structurally distinct from rigid fibrils. In addition, they proposed that an experimentally determined phase diagram matches the colloidal model predictions. On the other hand, they considered neither the critical concentration nor supersaturation of amyloid fibrillation. More recently, on the basis of kinetic simulation using explicit approach, Hall et al.<sup>82</sup> suggested possible regulatory effects that off-pathway processes might exert on the rate and extent of amyloid formation.

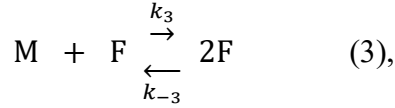
A long debated issue is whether oligomers or protofibrils represent on-pathway intermediates that must be populated along the pathway leading to fibril formation or off-pathway intermediates that are located at a dead end of the reaction scheme<sup>61</sup> (Fig. 1B). The competitive mechanism discussed above supports the off-pathway (or dead end) hypothesis. Sasahara et al. reported the complete disappearance of the transiently accumulated amorphous aggregates of hen egg white lysozyme or  $\beta$ 2m upon amyloid

fibrillation, suggesting that amorphous aggregates were also off-pathway products<sup>83,84</sup>. The distinct intermolecular  $\beta$ -sheet component in the infrared spectrum of the amorphous aggregates ( $1616\text{ cm}^{-1}$  vs.  $1620\text{-}1622\text{ cm}^{-1}$  in fibrils, Table 1) suggest a completely different structure and thus further supports the off-pathway hypothesis. On the other hand, many proteins have been shown to form on-pathway oligomers<sup>61</sup>. In cases in which oligomers, protofilaments or amorphous aggregates are off-pathway intermediates, fibrillation occurs only after they dissociate; however, the extent of the conformational change required to restart fibrillation remains largely unknown.

#### *Simulation of observed kinetics*

I simulated the salt-dependent competition of amyloid fibrillation and amorphous aggregation assuming Mechanism 1 (Fig. 6A). In our competitive mechanism, I assumed that all competing processes were reversible with the corresponding critical concentrations. I assumed that amorphous aggregates formed without a lag phase, which is in contrast to the nucleation-limited growth of fibrils<sup>43</sup>. Similar competitive and reversible mechanism has been reported for polymers from  $\pi$ -conjugated oligomers, in which two parallel and competing pathways explain the presence of a kinetically favoured intermediate assembly that forms quickly, but then transforms into a thermodynamically favoured form<sup>85</sup>. Similar to the competitive mechanism suggested by Miti et al.<sup>62</sup>, I assumed that our pathway of amorphous aggregation accommodated oligomers, curvilinear fibrils, and large amorphous aggregates, the interconversion of which was more rapid than supersaturation-limited amyloid fibrillation.

To analyze the kinetics of fibrillation on the basis of Mechanism 1, I used equations taken from the F-W model<sup>19</sup>:



$$K_1 = \frac{k_1}{k_{-1}} \quad (4),$$

$$K_2 = \frac{k_2}{k_{-2}} \quad (5), \text{ and}$$

$$K_3 = \frac{2k_3}{[M]k_{-3}} \quad (6),$$

where M is the monomeric protein, F is the amyloid fibril, AA is the amorphous aggregate,  $k_1$ ,  $k_{-1}$ ,  $k_2$ ,  $k_{-2}$ ,  $k_3$ , and  $k_{-3}$  represent the rate constants of the respective processes, and  $K_1$ ,  $K_2$ , and  $K_3$  represent the corresponding equilibrium constants. Although these equations considered neither the elongation of fibrils through the ends of fibrils nor the breakage of preformed fibrils leading to secondary nucleation, I considered them one of the minimal models reproducing the observed kinetics.

In order to fit the observed kinetics with the model, I estimated the equilibrium (i.e., final) fractions of fibrils, amorphous aggregates, and monomers at various salt concentrations. I assumed that 100% of the molecules transformed to amorphous aggregates at 1.0 M NaCl. The fractions of amorphous aggregates at various NaCl concentrations were then estimated from the ANS fluorescence intensity at 0.5 h, when fast amorphous aggregation finished. Analytical ultracentrifuge showed that, at concentrations greater than 0.2 M NaCl, most of the protein molecules precipitated at 3,000 rpm, confirming no significant residual monomers (data not shown). The fractions

of fibrils at concentrations greater than 0.2 M NaCl were then obtained by subtracting the fractions of amorphous aggregates from 1. Alternatively, the fractions of fibrils were estimated from the maximal ThT intensities at various NaCl concentrations, in which the ThT value at 0.2 M NaCl was used to obtain the specific ThT value of fibrils. In either method, the fraction of fibrils showed a maximum at 0.2 M NaCl while the fraction of amorphous aggregates increased at a higher NaCl concentration (Fig. 6B).

I fit fast kinetics within 0.5 h, assuming that equilibrium was rapidly established between unfolded monomers and amorphous aggregates. Formation and dissociation rate constants were determined in order to reproduce the fast kinetics and amount of amorphous aggregates at 0.5 h. I then fit the slow kinetics representing the formation of amyloid fibrils. At the respective NaCl concentrations, I assumed a factor relating the ThT fluorescence and ANS fluorescence of fibrils. The fit kinetics showed that the amount of amorphous aggregates exhibited a maximum, at moderate concentrations of salt (e.g. 0.2-0.3 M NaCl) and this was followed by a slow decrease coupled with the formation of amyloid fibrils. Since ANS fluorescence monitors both amorphous aggregates and amyloid fibrils, it exhibited a shoulder at 0.5 h (Fig. 5D, E).

The competitive mechanism sufficiently reproduced the observed kinetics at various NaCl concentrations monitored by ThT and ANS (Fig. 5). Both the equilibrium constants of amyloid nucleation ( $K_1$ ) (Fig. 6C) and amorphous aggregation ( $K_2$ ) (Fig. 6D) increased with higher NaCl concentrations. The equilibrium constant for elongation ( $K_3$ ) was relatively constant (Fig. 6E). However, since amyloid fibrillation was more favorable before amorphous aggregation became dominant, the maximum amount of fibrils was achieved at moderate concentrations of NaCl (Fig. 6B).

### *Free energy change of protein aggregation and phase diagram*

Although the detailed mechanisms of protein aggregation remain elusive<sup>19</sup>, a simplified model on the basis of the equilibrium of monomers and aggregated forms proposes the importance of the remaining monomer concentration  $[M]_c$ , which is often referred to as the "critical concentration"<sup>21,53,57,86,87</sup> because aggregates form when the concentration of monomers exceeds  $[M]_c$ . By determining  $[M]_c$ , I can calculate the free energy change in fibrillation or amorphous aggregation ( $\Delta G_{M-F}$  or  $\Delta G_{M-AA}$ ) by:  $\Delta G = -RT \ln K = RT \ln [M]_c$ , where  $R$  and  $T$  are the gas constant and temperature, respectively. Critical concentration is analogous to critical micelle concentration and is an important parameter independent of the complicated mechanisms of aggregation. Moreover, when I assume a phase transition between monomers and solid-like fibrils or amorphous aggregates,  $[M]_c$  simply represents the solubility of monomers.

The salt-dependent phase transitions of the major products, from monomers to amyloid fibrils to amorphous aggregates, can be illustrated by NaCl-concentration-dependent changes in the  $[M]_c$  values for amyloid fibrils and amorphous aggregates (Fig. 7). The logarithm of the  $[M]_c$  value is proportional to the standard free energy change in the phase transition (Fig. 7A). At NaCl concentrations lower than  $\sim 0.05$  M, the  $[M]_c$  values of amorphous aggregation and amyloid fibrillation were both higher than the experimental protein concentration ( $25 \mu\text{M}$  or  $0.3 \text{ mg/ml}$ ); therefore, the free energy changes of aggregation were positive (Region 1). Thus, monomers dominated in equilibrium. At a NaCl concentration between  $0.05 - 0.15$  M (Region 2a), the free energy change of amyloid fibrillation became negative while that of amorphous aggregation was still positive. Thus, only amyloid fibrillation occurred after a lag phase. At a NaCl concentration between  $0.15 \sim 0.3$  M (Region 2b); free energy change of amorphous

aggregation became negative. Since amorphous aggregation is rapid and amyloid fibrillation is slow, the rapid formation and slow relaxation of amorphous aggregation was coupled with the slow formation of amyloid fibrils (Fig. 7C). Only the rapid formation of amorphous aggregates occurred at a NaCl concentration above  $\sim 0.5$  M. Here, it is noted that Region 2 (amyloid fibrils) in the general phase diagram shown in Fig. 1A was divided into two subregions (Regions 2a and 2b) depending on the kinetics of fibrillation.

Moreover, salt-dependent changes in the fit rates and equilibrium constants of fibrillation and amorphous aggregation suggested the origin of the observed complicated kinetics (Fig. 6C-E). The increase in fibrillation equilibrium ( $K_1$ ,  $K_3$ ) was mainly caused by an elevated nucleation rate ( $k_1$ ) (Fig. 6C) without a significantly change in the elongation reaction (Fig. 6E). On the other hand, the increase in amorphous aggregation ( $K_2$ ) was caused by a decrease in the dissociation rate ( $k_{-2}$ ) (Fig. 6D).

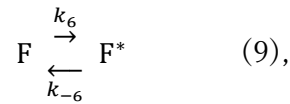
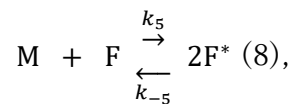
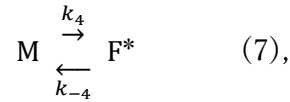
The observed kinetics of amyloid fibrillation also illustrate the conformational phase diagram, which is dependent on NaCl and protein concentrations (Fig. 7B). Although the linear dependencies of the free energy changes of amyloid fibrillation and amorphous aggregation with a crossing point at a high NaCl concentration predicted the disappearance of an amyloidogenic region at the low protein concentration and high NaCl concentration regions, the exact shape of the phase diagram under the extreme protein and salt concentrations remain unknown without exact data under those conditions. In this context, it is noted that a general phase diagram shown in Fig. 1A assumed the persistence of amyloidogenic region even at very high salt concentrations. Nevertheless, I argue that a conformational phase diagram common to various amyloidogenic proteins may be reproduced by a competitive mechanism between supersaturation-limited

amyloid fibrillation and unlimited amorphous aggregation.

*Ultrasonication-dependent decrease in ThT fluorescence*

In the cases of  $\alpha$ -synuclein<sup>68</sup> and A $\beta$  peptides<sup>67</sup>, extensive ultrasonication transformed preformed fibrils to amorphous aggregates with decreased ThT fluorescence, as confirmed by a CD spectroscopy and EM or AFM images. This was not the case for  $\beta$ 2m fibrils and fibrillar aggregates with reduced ThT fluorescence that retained amyloid-like  $\beta$ -structures. Similar aggregates were induced from  $\beta$ 2m monomers under extensive ultrasonic power (Figs. 2 and 3).

I now assume that extensive ultrasonication can produce a distinct conformational state located between amorphous aggregates and amyloid fibrils, which may be represented by F\* (Fig. 6F, Mechanism 2). I modified Mechanism 1 by adding an additional pathway producing F\* (Eqns. 7 and 8). I also assumed that the preformed fibrils (F) may be converted to (F\*) by extensive ultrasonication (Eqn. 9),



$$K_4 = \frac{k_4}{k_{-4}} \quad (10),$$

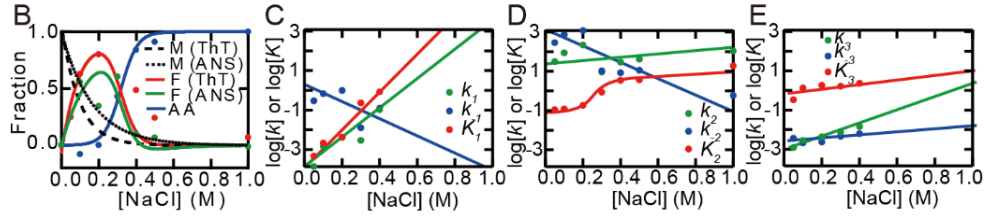
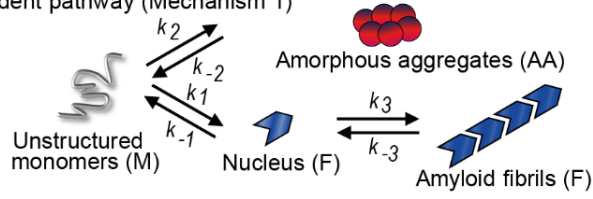
$$K_5 = \frac{2k_5}{[M]k_{-5}} \quad (11), \text{ and}$$

$$K_6 = \frac{k_6}{k_{-6}} \quad (12),$$

with these equations on the basis of Mechanism 2 (Fig. 6F), a series of kinetic data as

shown in Figure 2 were simulated, in which ultrasonic power varied at 0.1 M NaCl (Fig. 6G). Moreover, I analyzed a series of data obtained by So et al.<sup>44</sup> with a microplate, in which ultrasonic power varied depending on the wells of the microplate (Fig. 6H). In an analysis of ultrasonication-dependent reactions, I assumed that the rate ( $k_2$ , and  $k_{-2}$  (Eqn. 2)) and equilibrium constants ( $K_2$  (Eqn. 5)) of amorphous aggregates and those for elongation processes of amyloid fibrils ( $k_3$ , and  $k_{-3}$  (Eqn. 3) and  $K_3$  (Eqn. 6)) and amyloid-like fibrils ( $k_5$ ,  $k_{-5}$  (Eqn. 8) and  $K_5$  (Eqn. 11)) were the same as those obtained for stirring-dependent reactions at 0.1 M NaCl because they are unlikely to be significantly affected by ultrasonication<sup>43</sup>.

A Salt-dependent pathway (Mechanism 1)



F Ultradronication-dependent pathway (Mechanism 2)

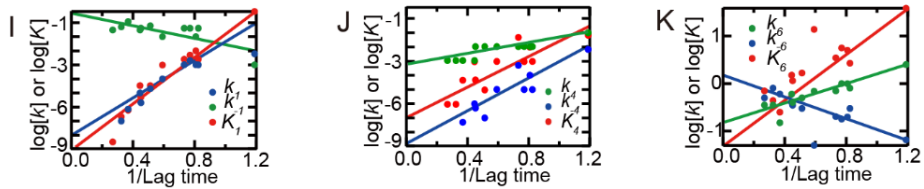
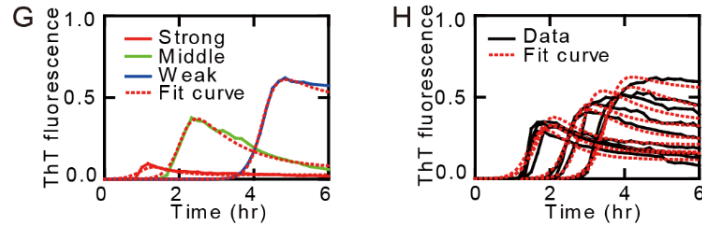
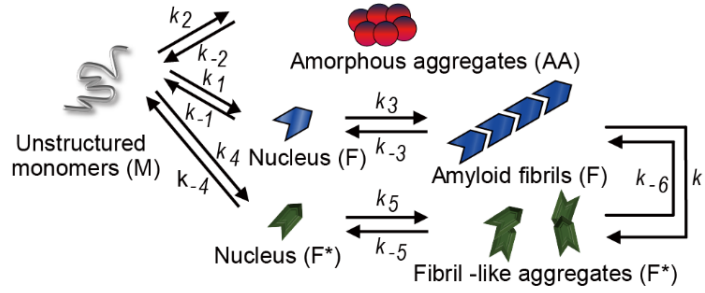


**Figure 6.** Analysis of the NaCl concentration and the ultrasonic power dependence of amyloid fibrillation by a competitive mechanism. (A) The competitive mechanism of amyloid fibrillation and amorphous aggregation. (B) Dependencies on the NaCl concentration of the fractions of monomers, fibrils, and amorphous aggregates. (C-E) Dependence on the NaCl concentration of the rate constants and equilibrium constants on the basis of Mechanism 1. (C)  $k_1$ ,  $k_{-1}$ , and  $K_1$ . (D)  $k_2$ ,  $k_{-2}$ , and  $K_2$ . (E)  $k_3$ ,  $k_{-3}$ , and  $K_3$ . (F) The competitive mechanism of amyloid fibrillation and amorphous aggregation including fibril-like aggregates  $F^*$ . (G, H) Fitting of fibrillation kinetics under various levels of ultrasonic power by the competitive mechanism. (G) Experimental data were the same as those shown in Fig. 2A. (H) Experimental data were taken from So et al.<sup>44</sup>. (I-K) Dependencies on the NaCl concentration of rate constants and equilibrium constants on the basis of Mechanism 2. (I)  $k_1$ ,  $k_{-1}$ , and  $K_1$ . (J)  $k_4$ ,  $k_{-4}$ , and  $K_4$ . (K)  $k_6$ ,  $k_{-6}$ , and  $K_6$ . Other rate and equilibrium constants were assumed to be the same as those at 0.1 M NaCl without ultrasonication. Lines are guides for the eye. This figure is reproduced from Adachi, M. et al. 2015 with permission<sup>69</sup>.

All the observed kinetics were reproduced successfully, suggesting that the competitive mechanism was also useful for explaining the dependence on ultrasonic power of the kinetics monitored by ThT; however,  $\beta$ 2m retained an amyloid-like  $\beta$  structure even after extensive ultrasonication. Under the conditions of stronger ultrasonic power, the population of fibrils decreased while that of modified fibrils became dominant because the modified fibrils were favored kinetically and the preformed fibrils transformed to modified fibrils by extensive ultrasonication (Fig. 6G, H). The possible free energy profile and phase diagram for the formation of F\* fibrils under the conditions of extensive ultrasonication are illustrated in Figure 7A, B.

The inverse of lag time was considered to represent ultrasonic power.  $K_1$ ,  $k_1$ , and  $k_{-1}$  (Fig. 6I),  $K_4$ ,  $k_4$ , and  $k_{-4}$  (Fig. 6J), and  $K_6$ ,  $k_6$ , and  $k_{-6}$  (Fig. 6K) were then plotted against the inverse of lag time. The parameters obtained suggested that the combined effects of the equilibrium and rate toward the formation of F\* explain the accumulation of F\* under stronger ultrasonic powers. Although the significance of the respective rate constants still remains unclear, I adequately reproduced the change in the kinetics of fibrillation on the basis of competition between the parallel pathways (Fig. 6F).

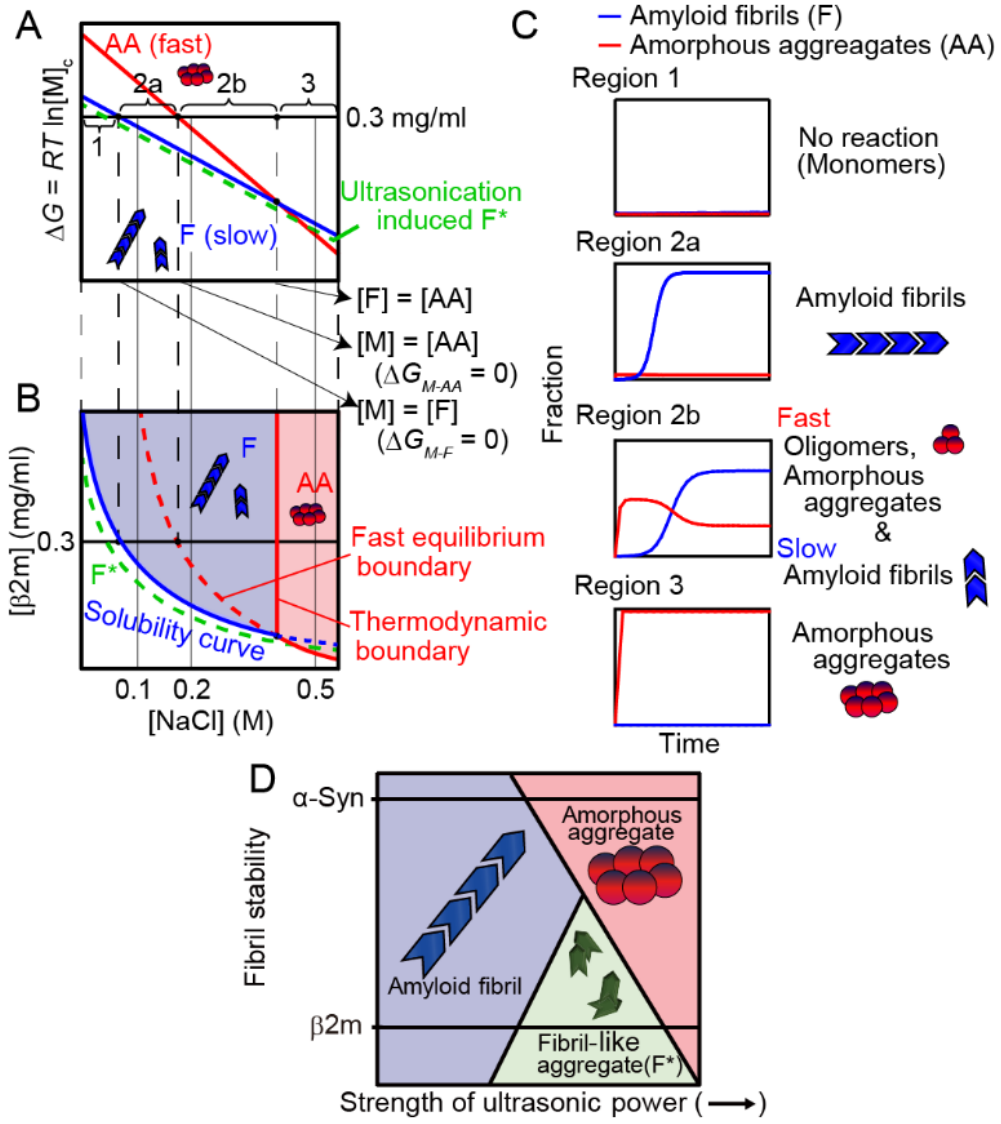


**Figure 7.** Competitive mechanism of supersaturation-limited and unlimited reactions. (A) Dependencies on the NaCl concentration of free energy changes of amyloid fibrillation and amorphous aggregation. The solid horizontal line indicates free energy changes for phase transitions at the  $\beta$ 2m concentration (25  $\mu$ M). Region 1: Critical concentrations for fibrillation and amorphous aggregations were higher than the  $\beta$ 2m concentration in the solution. Region 2a: Critical concentrations for fibrillation and amorphous aggregations were lower and higher, respectively, than the  $\beta$ 2m concentration. Region 2b: Critical concentrations for fibrillation and amorphous aggregations were both lower than the  $\beta$ 2m concentration, with the former being lower than the latter. Region 3: After the crossing point, the critical concentration of amorphous aggregation was lower than that of fibrillation and, thus, determined the overall kinetics. (B) The protein concentration- and NaCl concentration-dependent phase diagram of conformational states. The dotted green lines in (A) and (B) indicate the possible free energy profile and phase boundary, respectively, for the transition from monomers to F\* fibrils under the conditions of extensive ultrasonication. (C) Representative kinetics under Regions 1-3 are illustrated. (D) Dependence of the effects of ultrasonication on the stability of amyloid fibrils. Stable fibrils like those of  $\beta$ 2m produced partially destructed fibrillar aggregates whereas less stable  $\alpha$ -synuclein fibrils exhibited two-state destruction by ultrasonic irradiation. This figure is reproduced from Adachi, M. et al. 2015 with permission<sup>69</sup>.

## 2.5 Conclusion

Competition between crystallization and glass-transition has been elaborated for understanding the mechanism of protein folding<sup>88-90</sup>, in which the folding temperature ( $T_f$ ) corresponded to the temperature of crystallization and the glass transition temperature ( $T_g$ ) resembled the temperature of amorphous aggregation in which molecules were trapped in various local minima. To achieve cooperative and rapid protein folding, the temperature of glass transition should be markedly lower than the folding temperature in order to construct a smooth folding funnel with minimal frustration. An analogy of protein phase transition into crystal-like amyloid fibrils and amorphous aggregates appear to be valid. In the case of salt-dependent fibrillation, the critical concentrations of amyloid fibrils and amorphous aggregates (or oligomers) correspond to the folding temperature and glass transition temperature, respectively. To achieve cooperative amyloid fibrillation, two critical concentrations need to be markedly separated. However, for larger denatured proteins, the critical concentration of amorphous aggregation was close to that of fibrillation, making amyloid fibrillation difficult. In other words, the free energy balance between amyloid fibrils and amorphous aggregates determines their final distributions.

In addition, the current analysis argued the importance of supersaturation. Although I approximated amyloid fibrillation by a nucleation and growth mechanism, supersaturation is often too rigid to be broken under quiescent conditions. One possibility underlying spontaneous fibrillation under labile region is that supersaturation-unlimited amorphous aggregates gradually develop with an increase in the driving force of precipitation (e.g. NaCl concentration), thereby providing the seed-competent structures and ultimately breaking otherwise persistent supersaturation.

Finally, although oligomers are important targets of protein aggregation, I could

not focus on them because I did not isolate them clearly. Characterizing the exact role of oligomers in the context of the competitive mechanism will be important for further clarifying the general mechanism of protein aggregation.

Chapter 3. Comprehensive understanding of heat- and salt-dependent protein aggregation based on the supersaturation-limited competitive mechanism

### 3.1 Introduction

In general, it is known that proteins form amorphous aggregates at high temperature as represented by boiled egg. Recently, many human diseases that are caused by accumulation of protein aggregates have been found. There are two types of aggregates, the amyloid fibrils with highly ordered  $\beta$ -sheet structures and amorphous aggregates without no ordered structure<sup>6</sup>. The various aggregation models have been reported aiming to not only understand the underlying molecular mechanism, but also to accomplish the therapeutics of diseases by controlling the protein aggregation<sup>19,91-93</sup>. However, most of studies did not consider participation of amorphous aggregates.

In the previous chapter, with  $\beta$ 2m, I showed that amyloid fibrillation and amorphous aggregation compete depending on the surrounding conditions, such as irradiation of ultrasonication with different strength or salt-concentration<sup>69</sup>. This competitive mechanism could be explained by adopting the concept of supersaturation. As it is broadly known, a term of supersaturation is often used in the field of crystallography. However, in the field of protein science, Yoshimura et al. proposed that amyloid fibrils and amorphous aggregates possess the features of crystal-like and glass-like, respectively<sup>43,56,69</sup>. Therefore, the solubility limit is likely an important key factor for the competitive aggregation mechanism. In order to establish the generality of this mechanism, it will be important to reveal that the aggregation occurs competitively under various conditions.

In this chapter, I focused on the effects of temperature because it has been believed that protein aggregation is accelerated upon increasing temperature. However, this belief is complicated by the denaturation of native proteins at the high temperature, resulting in enhancement of hydrophobic interactions. During my study, I recognized that

the heat effects on protein aggregates, such as amyloid fibrils and amorphous aggregates were not clearly shown. Therefore, I expected to elucidate the generality of competitive aggregation mechanism, by illustrating the temperature-dependence of aggregation. In this chapter, I particularly focused on heating rate as a factor of determining protein aggregation.

In fact, the effects of temperature on protein aggregation have been studied widely, with keeping a boiled egg as a typical image of heat-induced protein aggregation. Furthermore, in our group, heating effects on protein aggregation were investigated by using calorimetry methods, such as ITC and DSC<sup>57,83,94-96</sup>. From these reports, formation and degradation of amyloid fibrils occurred depending on temperature: it occurred not only at high temperature but also at low temperature, resulting in so called “cold denaturation”, similar to that of native proteins<sup>97</sup>. However, the relationship between the amyloid fibrils and amorphous aggregates upon heating has not been investigated. I assumed that considering the roles of amorphous aggregates in the temperature-dependent aggregation of proteins will be useful for extending the competitive mechanism of protein aggregation.

Therefore, in this report, I focused on the heating effects on competitive protein aggregation between amyloid fibrils and amorphous aggregates, in order to elucidate general protein aggregation mechanism.

### 3.2 Materials and methods

#### *Protein and chemicals*

A recombinant human  $\beta$ 2m protein with an additional methionine residue at the N terminus was expressed in *Escherichia coli* and purified as previously reported<sup>70</sup>. Thioflavin T (ThT) was obtained from Wako Pure Chemical Industries, Ltd. (Osaka, Japan). All other reagents were purchased from Nacalai Tesque (Kyoto, Japan).

#### *Protein aggregation by heating*

Lyophilized  $\beta$ 2m was dissolved in 10 mM HCl. The concentration of  $\beta$ 2m was determined spectrophotometrically using a molar extinction coefficient of  $19,300 \text{ M}^{-1} \text{ cm}^{-1}$  at 280 nm based on its amino acid composition. The sample solution of 2.5 mL in a glass cuvette with a 1-cm light path contained 8.5  $\mu\text{M}$   $\beta$ 2m, 5  $\mu\text{M}$  ThT, 10 mM HCl and various concentrations of NaCl. Protein aggregation was detected by ThT fluorescence with an excitation wavelength of 445 nm and emission wavelength of 485 nm using Hitachi fluorescence spectrophotometer F4500 (Tokyo, Japan). Light scattering of 445 nm was also measured in order to detect the amorphous aggregation simultaneously with detecting ThT fluorescence. All fluorescence measurements were performed under stirring using magnetic stirring bar. The stirring speed was 800 rpm.

Heating rate was controlled by using peltier element (NIPPON TECMO CO., LTD.) during detecting the aggregation, and I measured the direct sample temperature by using thermocouple (ANRITSU METER CO., LTD.).

#### *Detection of degradation of amyloid fibrils*

In order to investigate the stability of amyloid fibrils that formed under the presence of various NaCl concentration, I obtained the pre-formed amyloid fibrils using Hitachi fluorescence spectrophotometer F4500 (Tokyo, Japan) at 25 °C with stirring using

stirring bar. The sample composition was the same as those of fluorescence measurements. The 300  $\mu\text{L}$  of pre-formed sample was used for heating measurements by using CD detecting the MRE 220 nm value. Then, it was expressed as the normalized value to calculate the progress of heat-dependent conformational transition.

#### *Detection of dissolution of amorphous aggregates*

The dissolution of amorphous aggregates could be detected by measuring the decreasing in light scattering by using a Hitachi fluorescence spectrophotometer F4500 (Tokyo, Japan) and a heating control device (Fig.1 A). In this study, amorphous aggregates could be obtained by incubation at 25  $^{\circ}\text{C}$  for 30 min with stirring in fluorescence spectrophotometer in the presence of high NaCl concentration ( $>1.0$  M). Then, heating was started at 1  $^{\circ}\text{C}/\text{min}$  to induce the dissolution of amorphous aggregates. The change in light scattering value was monitored to obtain the  $T_m$  value.

#### *CD measurements, AFM measurements*

Far-UV CD measurements were performed by using Jasco J820 spectropolarimeter (Tokyo, Japan). A quartz cuvette with 1 mm path length was used for measuring the CD spectra, and the results were expressed as mean residue ellipticity [ $\theta$ ]. A quartz cuvette with 10 mm path length was used for detecting the MRE of 230 nm value with heating under stirring with stirring bar. The stirring speed was 800 rpm. For this measurement, the sample volume was 2 mL, containing 8.5  $\mu\text{M}$   $\beta_2\text{m}$ , 10 mM HCl and various concentrations of NaCl: These were the same composition as used for the fluorescence measurements.

AFM measurements were performed by using AFM5100N (HITACHI, Tokyo, Japan). The volume of 20  $\mu\text{L}$  was taken from samples after the fluorescence or CD measurements and dropped on to mica plate. Then, the water was absorbed by using a

paper to dry the plate, after that, washed away 3 times by using distilled water.

### 3.3 Results

#### *Temperature-dependence of amyloid fibrillation and aggregation*

First, I investigated the dependence of  $\beta$ 2m aggregation on temperature. In order to control the heating rate, I constructed a heating-rate control device by using peltier element in fluorescence cell holder (Fig.1 A). Amyloid fibrillation was measured by ThT fluorescence at 485 nm with 0.2 °C/min heating. I simultaneously measured the light scattering at 445 nm to monitor the amorphous aggregation. From these measurements, I could detect distinct differences between amyloid fibrillation and amorphous aggregation. Furthermore, in order to obtain more information, CD measurements were performed by taking sample out from solution of fluorescence measurements at desired time points.

At first, amyloid fibrillation was observed under the standard conditions (8.5  $\mu$ M  $\beta$ 2m, 0.1 M NaCl, 5  $\mu$ M ThT, 10 mM HCl at 25 °C with stirring) without heating (Fig.1 B, C). The increase in ThT and LS intensity occurred simultaneously. Under these conditions, the lag time was around ~3 hours and elongation reaction finished at ~5 hours. These results were consistent with those monitored by the change in secondary structure measured by CD spectra. However, no aggregation occurred in the absence of NaCl: No increase in neither ThT nor light scattering was observed with 0.2 °C/min heating (Fig.1 D). CD spectra also showed that the structure of  $\beta$ 2m remained unfolded (Fig.2 E, F).

In the presence of 0.1 M NaCl, both of ThT and LS intensities increased at certain temperature (Fig.1 G). It was considered that amyloid fibrillation mainly occurred under these conditions. However, decrease in ThT was observed by continuous heating at high temperature. This decrease suggested degradation of amyloid fibril. Indeed, the change in the MRE value at 200 nm indicative of  $\beta$  structure component of  $\beta$ 2m amyloid fibrils gradually reduced with heating (Fig.1 H, I). However, a large amount of amyloid fibrils

was observed in AFM image of Fig.1 G inset, although the AFM image was taken after cooling. Therefore, it was not clear whether degradation of amyloid fibrils occurred at high temperatures.

In the presence of 1 M NaCl, amorphous aggregation occurred rapidly accompanied by an increase in light scattering, and this results consistent with previous study that investigated salt-concentration dependence<sup>43,69</sup> (Fig.1 J). Then, I observed that light scattering decreased with increasing temperature. Unexpectedly, increasing in ThT fluorescence was observed beginning around 45 °C. Thus, it was assumed that amyloid fibrils formed accompanied by dissolution of amorphous aggregates. However, CD measurements did not show typical spectra of amyloid fibrils: It was likely that amorphous aggregates disturbed the correct CD measurements (Fig.1 K, L). AFM image also showed that coexisting of amyloid fibrils and oligomer-like or amorphous-like structure.

From these results, it seemed important to verify heat-induced degradation of amyloid fibrils, a transition of fibrils to monomers, at moderate salt concentrations, and heat-dependent dissolution of amorphous aggregates followed by amyloid fibrillation.

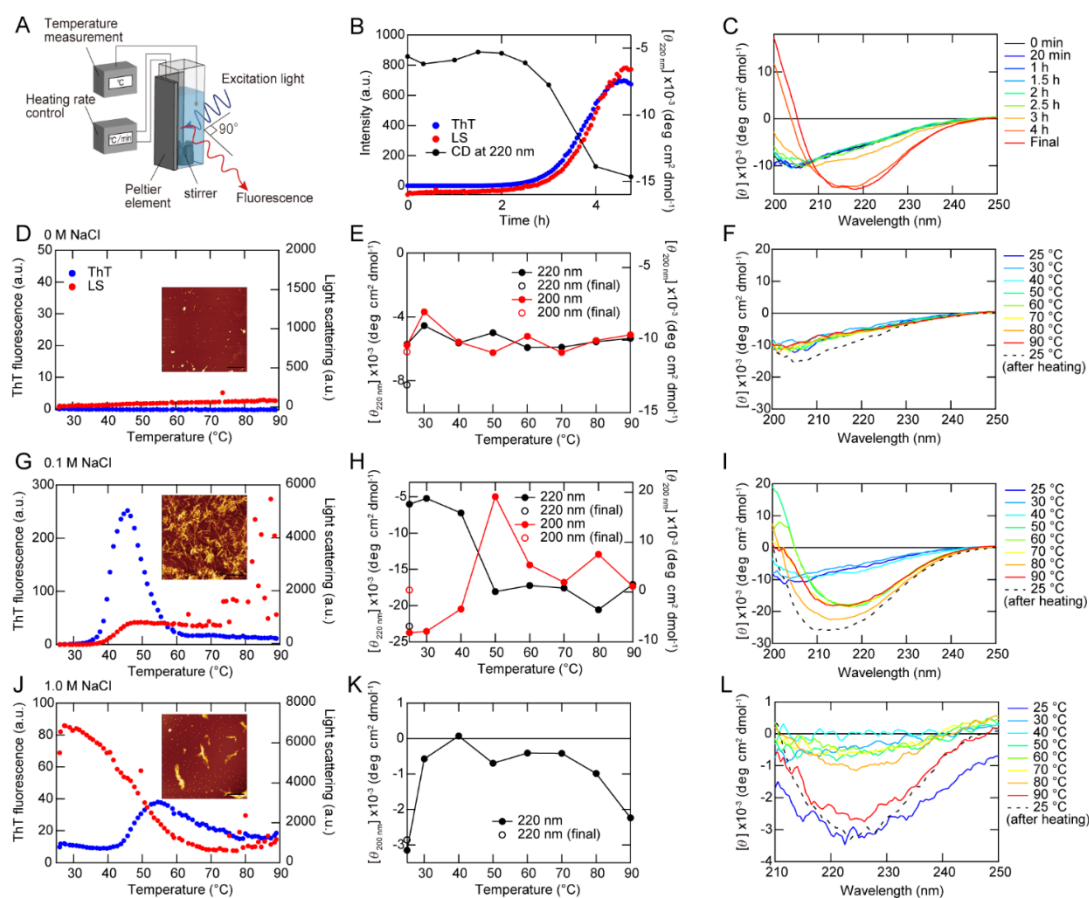


**Figure 1.** Heating-dependent conformational transitions of  $\beta$ 2m aggregation. (A) Scheme of heating-rate control device. (B) Amyloid fibrillation at 25 °C by measuring ThT fluorescence, light scattering and MRE value at 220 nm obtained from Fig.1 C. (C) CD spectra of Fig.1 B at respective time points. (D-F) Aggregation upon heating at 0.2 °C/min by measuring ThT fluorescence, light scattering and MRE value at 220 nm and 200 nm under the condition of 0 M NaCl, (G-I) 0.1 M NaCl, (J-L) 1.0 M NaCl. AFM images showed the morphologies after heating measurement at room temperature. The scale bar represented 1  $\mu$ m.

### *Degradation of amyloid fibrils with heating*

It has been assumed that amyloid fibrils are greatly stable under physiological conditions<sup>3,98</sup>. However, as described above, it was indicated that degradation of amyloid fibrils occurred upon heating. Therefore, in order to investigate the stability of amyloid fibrils, pre-formed amyloid fibrils that made under the conditions of various NaCl concentrations at 25 °C (Fig.1 B, presence of 100 mM NaCl) were heated at 0.5 °C/min accompanied by the CD measurement at 220 nm (Fig.2 A).

The CD measurements confirmed degradation of amyloid fibrils at a certain temperature, and this temperature was dependent on salt concentration (Fig.2 A). Furthermore, AFM images showed that morphology of amyloid fibrils that observed before heating (Fig.2 E) disappeared after heating (Fig.2 F). CD spectra also showed that pre-formed amyloid fibrils,  $\beta$ -rich spectra, were degraded to an unfolded state at 100 °C, and this changing was observed at each salt-concentration (Fig.2 B-C). From these results, it was demonstrated that amyloid fibrils could be degraded at high temperature and the stability of fibrils was greatly dependent on salt concentration. Indeed, at NaCl concentrations lower than 50 mM, for example 25 mM NaCl, amyloid fibrillation was not observed even incubation at 25 °C, ~12 h (data not shown). On the other hand, above 100 mM NaCl, for example 200 mM NaCl, I could not observe the degradation of amyloid fibrils because degradation temperature was probably higher than 100 °C. These results indicated that amyloid fibrils could be degraded at the low and high temperatures. In other words, I observed “cold denaturation” and “heat denaturation” of amyloid fibrils<sup>96</sup>.

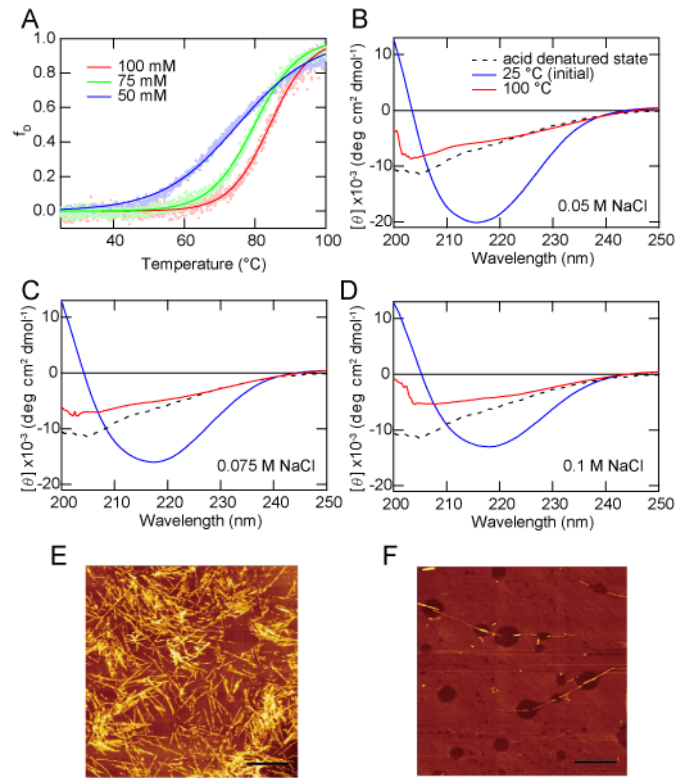


**Figure 2.** Degradation of amyloid fibrils by heating. (A) The denaturation curves of amyloid fibrils that formed in the presence of 100 (red), 75 (green) or 50 (blue) mM NaCl. (B-D) CD spectra of each sample at 25 °C (blue), 100 °C (red) and denatured state (dashed line). (E, F) AFM images of amyloid fibrils that formed in the presence of 100 mM NaCl (E), and after heating (F). The scale bar represented 1  $\mu\text{m}$ .

### *Dissolution of amorphous aggregates upon heating*

In the previous study, I reported that amorphous aggregates formed in the presence of high salt concentrations due to salting-out effect<sup>69</sup>. However, I observed the dissolution of amorphous aggregate as revealed by decreasing in light scattering (Fig.1 J). Furthermore, I observed the transition of amorphous aggregate to amyloid fibrils. I investigated these phenomena in detail.

At first, it was required to obtain the pre-formed amorphous aggregates. Therefore, I prepared amorphous aggregates at a high salt concentration. Then, after finishing the amorphous aggregation, heating the solution started at 1 °C/min (Fig.3 A). Decrease in light scattering was observed upon heating. Then, amyloid fibrillation occurred at a certain temperature represented by increasing in ThT fluorescence. AFM images also showed that amorphous aggregates that formed after 30 min at 25 °C (Fig.3 B left) transformed into amyloid fibrils (Fig.3 B right). Therefore, stability of amorphous aggregates also had salt-concentration dependence similar to amyloid fibrils. I analyzed the light scattering curves by fitting of sigmoidal curve, and obtained the half temperature ( $T_m$ ) (Fig.3 C, D). Then, it was demonstrated that the temperature of dissolution of amorphous aggregates was dependent on salt-concentration (Fig.3 D). However, it was considered that the value of  $T_m$  was not precise because of apparent decrease in light scattering in the presence of NaCl concentration above 1.6 M. This drastic decrease in light scattering was likely caused by very large aggregates under high salt conditions. It was empirically understood that the large aggregates tend to float to liquid surface, preventing precise detection. Furthermore, I could detect the increasing in ThT fluorescence in the concentration range NaCl from 0.9 M to 1.4 M (Fig.3 E). These results

showed that amorphous aggregates had the potential of transform into amyloid fibrils in the certain range of NaCl concentration.

Taken these results together, I could obtain the relationship between NaCl concentration and temperature against protein aggregation (Fig.3 F). It was able to understand distinctively amorphous dominant region and amyloid dominant region. Furthermore, it was noted that amorphous aggregates have a potential to transform into amyloid fibrils, as more stable aggregated state before dissolving into monomers. This novel point of view revealed that it is not always the case that denatured proteins form aggregates at high temperature.

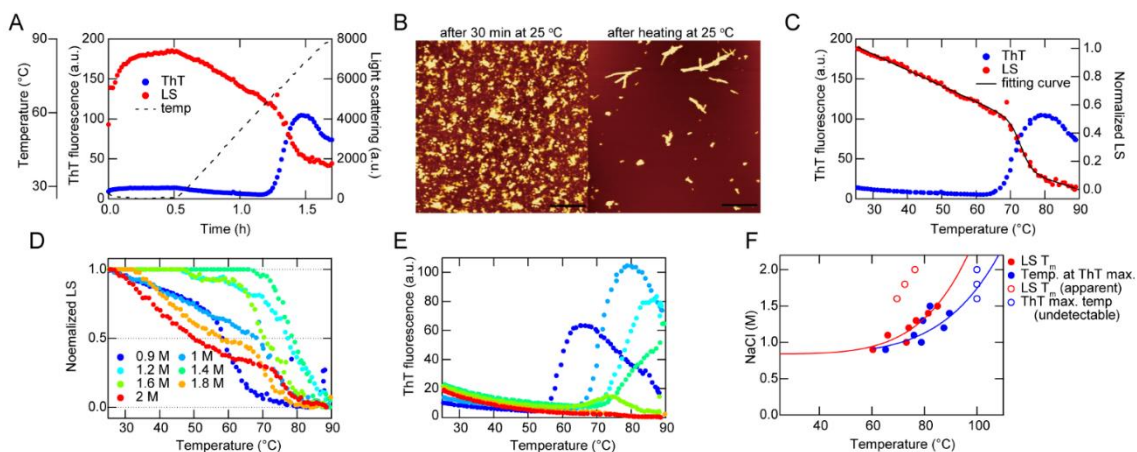


**Figure 3.** Dissolution of amorphous aggregates upon heating. (A) The kinetics of amorphous aggregation at 25 °C during 30 min were observed by measuring ThT fluorescence and light scattering, and representative figure obtained in the presence of 1 M NaCl. Then, the solution was heated at 1 °C/min to observe the dissolution of amorphous aggregates. (B) AFM images showed that amorphous aggregates that formed at 25 °C after 30 min (left), and after heating (right) in the presence of 1 M NaCl. The scale bar represented 1  $\mu$ m. (C) The changing in ThT fluorescence and normalized light scattering with heating extracted from Fig.3 A. The horizontal axis represented temperature. The black curve showed that fitting curve to obtain the  $T_m$  of amorphous aggregates. (D) The changing in normalized light scattering and (E) ThT fluorescence with heating in the presence of various NaCl concentrations. (F) The relationship between NaCl concentration and temperature for protein aggregation. The solid red circle represented  $T_m$  of light scattering and blue solid circle represented the temperature when reach ThT maximum intensity. The open circle represented apparent value because it could not detect in precisely.

### *Heating rate dependence of protein aggregation*

Up to here, I discussed that transition of amyloid fibrils into monomer or transformation of amorphous aggregates into amyloid fibrils with heating. Meanwhile, it was needed to investigate the transformation of monomer into amyloid fibrils to reveal the heat-dependent protein aggregation mechanism. Therefore, in this section I performed the measurements of changing in heating rate to investigate starting temperature of amyloid fibrillation.

I have already investigated that amyloid fibrillation at heating 0.2 °C/min as shown in Fig. 1. Here, I measured protein aggregation kinetics in detail at various heating rates: representative data in 0.1 M NaCl was shown in Fig. 4A-C. As noted in Fig. 4A, I could not observe the dramatic increase in ThT fluorescence and light scattering at heating 0.5 °C/min. This result indicated that heating rate was too fast to form the amyloid fibrils. On the other hand, amyloid fibrillation occurred at heating 0.2 and 0.1 °C/min at the certain temperature. Therefore, I obtained the transition temperature of monomer to amyloid fibrils by calculating the lag time. In this study, lag time was defined to be the time when ThT intensity reached 10 % of maximum. Figure 4 D showed the dependence of the lag time on the NaCl concentration and temperature. If heating rate was slower, the temperature of starting amyloid fibrillation became lower. However, there was almost no difference between 0.2 and 0.1 °C/min, and it might be expected that transition boundary of monomer to amyloid fibril existed in these regions. It was noted that the NaCl concentration above 0.3 M, the temperature at lag time became higher. This is because that amorphous aggregation, as competitive species against amyloid fibrils, occurred from these NaCl concentrations. These results at various temperatures were consistent with

previous reports that investigated the NaCl concentration dependence of protein aggregation at 37 °C<sup>43,69</sup>.

In addition to above results, I also investigated the heating-rate dependence of aggregation by using CD spectrometry. Representative results are shown in Fig. 4E, F, H, I. In the presence of 75 mM NaCl, amyloid fibrillation occurred at around 45 °C and heating rate of 0.3 °C/min. Under the condition of 0.5 °C/min, a slight amyloid fibrillation also occurred at higher temperature because of the increase in heating rate (Fig. 4E). However, unfolded state remained even at high temperature under the heating condition of 1 or 2 °C/min. This features were also shown the CD spectra (Fig. 4F). On the other hand, in the presence of 0.3 M NaCl, amyloid fibrillation occurred at any heating rate (Fig. 4H). Although maximum MRE value was different for each sample during heating measurement, all of the final CD spectra showed a typically  $\beta$ -sheet rich amyloid fibril spectrum (Fig. 4I). From these results, under the condition of relatively low NaCl concentration, it was considered that amyloid fibrillation could not occur at fast heating rate. The temperature increase was considered too fast to form the amyloid fibrils. In addition, the temperature reached to that of the degradation before forming amyloid fibrils. Meanwhile, under the condition of relatively high NaCl concentration such as 0.3 M NaCl, amyloid fibrillation could occur even under a fast heating rate because amyloid fibrils were stable at high temperature (Fig. 4G). This showed that heat denaturation of amyloid fibrils formed in the presence of 0.3 M NaCl.

Taken together, I showed the temperature of amyloid fibrillation and degradation by investigating the heating rate dependence of aggregation.

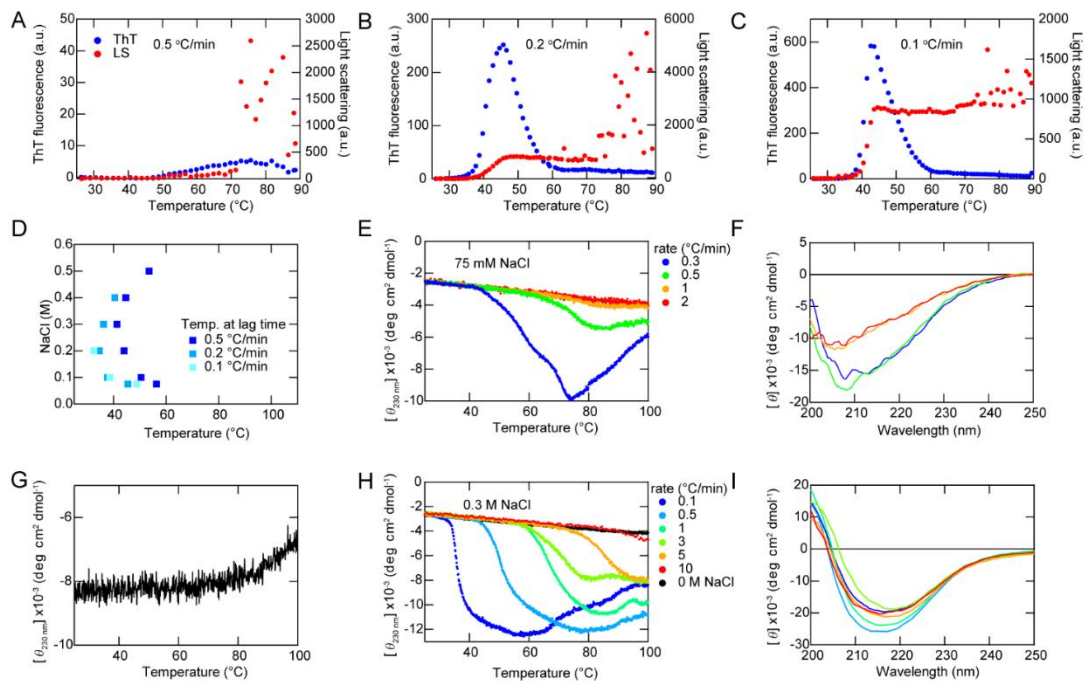


**Figure 4. Heating rate dependence of protein aggregation to investigate the transition of monomer into amyloid fibrils.** (A-C) Fluorescence measurements of heating rate dependence of protein aggregation heating at 0.5 (A), 0.2 and 0.1 °C/min under the presence of 0.1 M NaCl. (D) The temperature at lag time of each samples were plotted against NaCl concentration and temperature. (E, F) CD measurements of heating rate dependence of protein aggregation in the presence of 75 mM NaCl by using 1-cm cuvette with stirring 800 rpm and monitored the 230 nm of MRE value (E). CD spectrum of each sample after heating at 25 °C was shown in (F). (G) The stability of amyloid fibrils that formed in the presence of 0.3 M NaCl at 25 °C. (H, I) The same experiment as (E,F) was performed in 0.3 M NaCl.

### 3.4 Discussion

#### *Effects of temperature on protein aggregation*

I investigated that the effects of temperature on protein aggregation, particularly amyloid fibrils and amorphous aggregates. Although it is widely considered that protein aggregation tends to occur at high temperature, this study suggested that both types of aggregates could be dissociated even if aggregates formed under lower temperatures. Furthermore, the transition of amorphous aggregates into amyloid fibrils was observed at the certain range of temperature and salt concentrations. These phenomena of protein aggregation against temperature provide a new insight into structural properties of proteins.

I summarized the results that obtained in this study as a phase diagram showing the relationship between NaCl concentration and temperature (Fig. 5). The temperatures at the lag time of amyloid fibrillation that obtained in the heating experiments (Fig. 4) were plotted as filled square symbols (Fig. 5A). These points indicated the temperature where amyloid fibrillation mainly started. However, it is noted that the lag time was dependent on NaCl concentration and temperature. In other word, even under the region below the blue area in Figure 5A, amyloid fibrils had the potential to form after a prolonged period. In the previous studies, it was also reported that amyloid fibrils of  $\beta 2m$  formed in the presence of 0.1~0.3 M NaCl<sup>43,46,69</sup>. Therefore, although it was expected that region of amyloid fibrils expand to those of lower salt concentration in Figure 5A, I believe that the profile of amyloid fibrils against temperature did not differ from the current results. On the other hand, amyloid fibrils were degraded by heating at higher temperature, and  $T_m$  was plotted as triangle symbols in Figure 5A. Then, it was demonstrated that this  $T_m$  value was dependent on the NaCl concentrations. Therefore, it

was considered that amyloid fibrils were stabilized by increasing the NaCl concentration. Taken these results together, I described a U-shaped curve for the boundary between unfolded monomer and amyloid fibrils (Fig. 5A). Furthermore, it should be noted that the temperature at the lag time shifted to a high temperature under the condition above 0.3 M NaCl compared with ~0.2 M. Above around this NaCl concentration, it was reported that amorphous aggregates accumulated as kinetically trapped species before starting the amyloid fibrillation<sup>69</sup>. Therefore, in this case, it could be expected that the delay of amyloid fibrillation occurs due to the transient amorphous aggregation (Fig. 5A dashed red curve).

Meanwhile, amorphous aggregation mainly occurred at NaCl concentration (Fig. 5B). The red circle symbols were plotted as  $T_m$  of amorphous aggregates that obtained by analyzing the light scattering results. From these results, it could be proposed that, although amorphous aggregates were dissociated at the relatively higher temperature, it became difficult in the presence of high salt concentration. In other word, stability of amorphous aggregates increased by increasing the concentration of NaCl, the same as amyloid fibrils. At very high NaCl concentrations, the robust amorphous aggregates formed due to strong salting-out effect. Furthermore, the blue circle symbols were plotted as the temperature of the ThT maximum intensity (Fig. 5B). These points indicated that amyloid fibrillation occurred after the amorphous aggregation at the high temperature. From previously reports, I understood that the relationship between amyloid fibrils and amorphous aggregates was the same as that of crystals and glasses<sup>43,69</sup>. Furthermore, it was considered that glass-like aggregates produce the scaffold for crystal growth. Therefore, it was considered that these phenomena were similar to crystal growth process:

Salting-out precipitates can give rise to highly order structures<sup>99</sup>, and it could understand as “Ostwald ripening” that is well known in the field of crystallography<sup>100</sup>.

Up to here, I showed that amyloid fibrils would form at high temperature even if the high salt concentration produced amorphous aggregation at ambient temperature. However, the temperature of amyloid fibril degradation was not clear under the high salt concentration. Because the temperature of formation amyloid fibrils was too high to investigate the melting  $T_m$  of fibrils. I believe that amyloid fibrils formed at high NaCl concentrations were also degraded at higher temperature. Therefore, I combined these results to understand the protein aggregation mechanism against temperature.

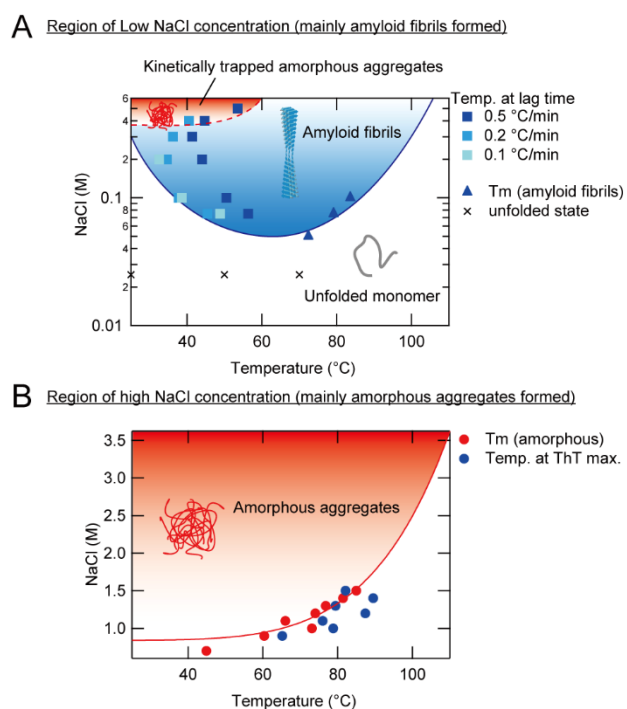


**Figure 5. The region of protein aggregation based on temperature and NaCl concentration.** (A) The region of low NaCl concentration was shown with a focus on amyloid fibrils. The filled blue square symbols indicated temperature at lag time of ThT fluorescence. Each color showed the differences of heating rate, shown in legend. The filled triangle symbols indicated the  $T_m$  value of amyloid fibrils. The crossing symbols indicated the unfolded state. These points were obtained by performing the experiments that investigated whether formation of aggregates occur or not at each temperature. (B) The region of high NaCl concentration was shown with a focus on amorphous aggregation. The red circle symbols indicated the  $T_m$  value of amorphous aggregates. The blue circle symbols indicated the temperature at the ThT maximum intensity.

### *Free energy change of protein aggregation and phase diagram*

In a previous study, I proposed that the competitive mechanism of protein aggregation<sup>69</sup>. There were equilibrium of unfolded monomers and aggregated forms, and I determined the free energy changes in amyloid fibrillation and amorphous aggregation against unfolded monomers ( $\Delta G_{M-F}$  or  $\Delta G_{M-AA}$ ) by  $\Delta G = -RT \ln K$ , where  $R$ ,  $T$  and  $K$  are the gas constant, temperature, and equilibrium constant between monomers and each aggregates, respectively. Furthermore, in the case of temperature-dependence of protein stability, I described the profile of  $\Delta G$  as U-shaped. Therefore, it is considered that aggregates have the heat denaturation point and cold denaturation point, similar to the native protein folding and unfolding. It is noted that the Ikenoue et al. reported the study of cold denaturation of  $\alpha$ -synuclein amyloid fibrils<sup>96</sup>. In order to understand the comprehensive protein aggregation mechanism, I combined the region of amyloid fibrillation and amorphous aggregation described above, illustrating the changing in free energy at the certain NaCl concentration (Fig.6).

At first, only amyloid fibrillation occurred in the presence of 100 mM NaCl (Fig. 6A). At this NaCl concentration, amyloid fibrils were more stable than unfolded state of  $\beta 2m$  below  $T_m$  temperature. Although it seems likely that amyloid fibrillation does not occur at low temperature in the phase diagram (Fig. 6A upper),  $\beta 2m$  has a potential to form amyloid fibrils at that region, as described above. Therefore, it was expected as amyloid fibrils were the most stable state even at low temperature. Degradation of amyloid fibrils occurred above the  $T_m$  temperature ( $\Delta G_{M-F} = 0$ ). However, alternative types of aggregates, amorphous aggregates could not form at this NaCl concentration due to the positive  $\Delta G_{M-AA}$  value (Fig. 6A lower).

Next, the region appears where amorphous aggregates accumulate as kinetically trapped state (Fig. 6B). As described above, the red dash curve indicated that amorphous aggregation occurred before amyloid fibrillation due to the delay of lag time compared with expected curve. In the presence of 400 mM NaCl, it was considered that amorphous aggregates formed kinetically up to around 40 °C. Therefore, red curve that represented the changing in  $\Delta G_{M-AA}$  was negative, and it was expected that amorphous aggregation disappeared at above the  $\Delta G_{M-AA} = 0$  (Fig. 6B upper). Similar to the condition of 100 mM NaCl, amyloid fibrils were most stable state at 400 mM NaCl. Therefore, amyloid fibrillation occurred up to the  $\Delta G_{M-F} = 0$ . Then, degradation of amyloid fibrils occurred above the  $T_m$  temperature ( $\Delta G_{M-F} = 0$ ) (Fig. 6B lower). However, this  $T_m$  point was not precisely determined of experimental difficulty.

Third, the region that amorphous aggregation is the thermodynamically most stable state appears (Fig. 6C). In the presence of 1 M NaCl, it has already been reported by my group that  $\beta 2m$  formed the amorphous aggregate as a stable state. In other words,  $\Delta G_{M-AA}$  (red curve) is the most negative at 1 M NaCl. However, it was a novel finding that, upon heating, dissolution of amorphous aggregates occurred and amyloid fibrils formed. From these results, I propose that there is a crossing point between  $\Delta G_{M-F}$  (blue curve) and  $\Delta G_{M-AA}$  (red curve) (Fig. 6C lower). Then, transformation of amorphous aggregates into amyloid fibrils occurred above the temperature of this crossing point. This phenomenon was similar to the transition of glass-like aggregates into crystals for native protein. From this point of view, I would like to emphasize that relationship between amyloid fibrils and amorphous aggregates for unfolded proteins are similar to that of crystal and glass states of native proteins. Finally, degradation of amyloid fibrils was expected at higher temperature ( $\Delta G_{M-F} = 0$ ).

Form these results, I explain the phenomena of protein aggregation with heating by considering three species, unfolded state, amyloid fibrils and amorphous aggregates. Each aggregate has the each critical concentration to form itself, and the critical point is dependent on surrounding conditions. Therefore, it is considered that there is a competitive mechanism of both types of aggregates even under various temperature and heating conditions.

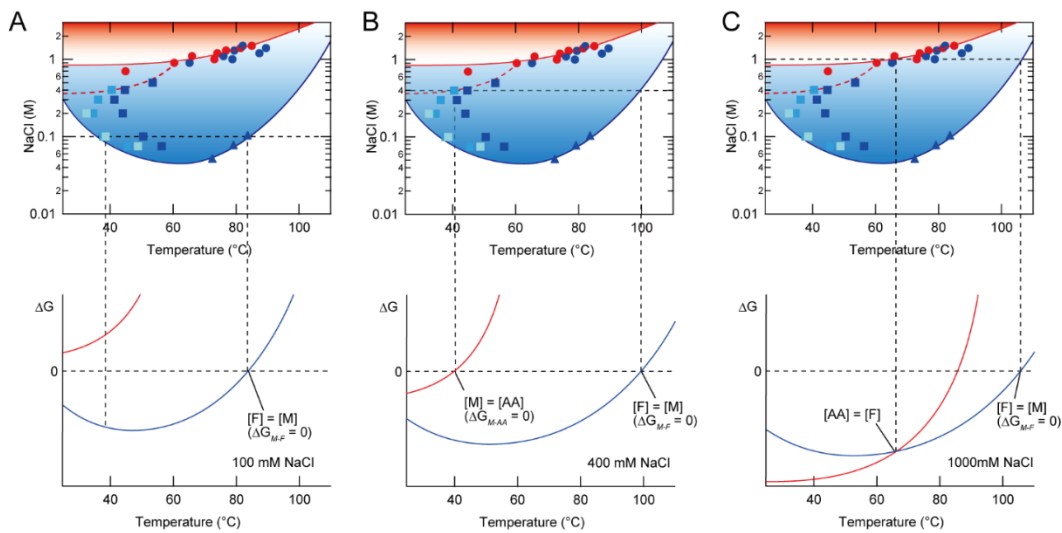


**Figure 6. The relationship between phase diagram and free energy change.** Upper figure of (A), (B) and (C) showed that phase diagram between NaCl concentration and temperature and the horizontal dashed line indicated that 100 mM NaCl (A), 400 mM NaCl (B) and 1000 mM NaCl, respectively. (C). Lower figure of (A), (B) and (C) indicated that the changing in  $\Delta G$  of amyloid fibrils (blue curve) and amorphous aggregates (red curve) in the presence of 100 mM NaCl, 400 mM NaCl and 1000 mM NaCl, respectively. The letter of “M” indicated the monomers, “F” indicated the amyloid fibrils and “AA” indicated the amorphous aggregates.  $\Delta G = 0$  was shown by dashed line. If the curve cross with this line, that point is the critical point.

### **3.4 Conclusion**

In this chapter, I focused on the effects of temperature on protein aggregation to investigate the generality of competitive aggregation mechanism between amyloid fibrils and amorphous aggregates. As the results, I found that the amyloid fibrils and amorphous aggregates had the close relationship each other even for heating. For example, the transition of amorphous aggregates into amyloid fibrils at high temperature was a representative result for demonstrating the competitive mechanism. Furthermore, it is interesting that both aggregates could be degraded at higher temperature for unfolded protein. It is widely considered as preconceived idea that protein aggregates formed at high temperature similar to boiled egg. Although the behavior of native proteins might differ from that of unfolded proteins, this study produced that proteins have properties of typical substances dissolved in water. Furthermore, I re-recognize that relationship between amyloid fibrils and amorphous aggregates was similar to crystals and glasses. Due to the kinetic and thermodynamic balance of amorphous aggregates and amyloid fibrils, they produce complicate kinetic behavior as represented by the concept of Ostwald ripening that kinetically trapped species transform to thermodynamically stable state.

## Chapter 4. General conclusion

In this study, I aimed to elucidate the protein aggregation mechanism, which is one of the most important topics in protein science. In order to accomplish this object, I focused on two main types of aggregates, amyloid fibrils and amorphous aggregates. Because there are obvious differences in structure, formation reaction, morphology, and methodologies to distinguish. It is no need to mention that there are many species of aggregates, such as oligomers, proto-fibrils, curvilinear, needle-like, noodle-like fibrils and so on. However, my point of view is to produce the general protein aggregation mechanism. Indeed, I obtained a series of evidence distinguishing amyloid fibrils and amorphous aggregates from this study through chapter 2 and 3.

In chapter 2, I investigated that salt-concentration dependence and ultrasonic-intensity dependence of protein aggregation. Although it was difficult to understand the effect of ultrasonication because new species was produced, the effect of salt became clear. From investigation of salt-concentration dependence, it was found that amyloid fibrils and amorphous aggregates have each critical concentration for formation because formed species was differ depending on salt concentration. At the certain range of salt-concentrations, amorphous aggregates formed by rapid reaction before amyloid fibrillation occurred. I discussed that these phenomena occurred because amyloid fibrils are supersaturation-limited and amorphous aggregates are unlimited species by adopting the concept of crystal and glass. Due to this relationship, I propose that protein aggregation occur competitively.

In chapter 3, I investigated the temperature-dependence of protein aggregation in order to elucidate the generality of competitive aggregation mechanism that was demonstrated in chapter 2. As a result, I obtained a phase diagram between NaCl concentration and temperature against protein aggregation. From this result, it was

demonstrated that each aggregate has critical concentration for aggregation and dissolution against temperature, which is similar to the salt-effects shown in chapter 2. Furthermore, it was found that both types of aggregates were dissociated at high temperature. In other word, I observed the reverse reaction of competitive aggregation mechanism. Finally, I explained the phenomena occurred by heating by adopting the competitive aggregation mechanism, combining the NaCl concentration dependence and temperature dependence. Thus, I established a comprehensive phase diagram dependent on salt and temperature effects.

Taken together these results, I propose the protein aggregation mechanism by focusing on the two type of aggregates. Furthermore, I found that many features were similar to the relationship between crystal and glass. For example, transition of amorphous aggregates into amyloid fibrils was representative results similar to crystal growth process governed by Ostwald ripening. Moreover, supersaturation play the key role for protein aggregation because this factor determined the aggregation type. In connection with this, critical concentration is the one of most important key words for understand the competitive protein aggregation mechanism. Taking these properties of protein aggregation into account, I discuss and understand the aggregation phenomena. Finally, I would like to conclude that this study produced the new insight against present complicated research field of protein aggregation.

## References

- 1 Anfinsen, C. B. Principles that govern the folding of protein chains. *Science (New York, N.Y.)* **181**, 223-230 (1973).
- 2 Hartl, F. U. & Hayer-Hartl, M. Converging concepts of protein folding in vitro and in vivo. *Nature Structural & Molecular Biology* **16**, 574, doi:10.1038/nsmb.1591 (2009).
- 3 Dobson, C. M. Protein folding and misfolding. *Nature* **426**, 884-890, doi:10.1038/nature02261 (2003).
- 4 Ellis, R. J. & Hartl, F. U. Principles of protein folding in the cellular environment. *Current opinion in structural biology* **9**, 102-110 (1999).
- 5 Amm, I., Sommer, T. & Wolf, D. H. Protein quality control and elimination of protein waste: the role of the ubiquitin-proteasome system. *Biochimica et biophysica acta* **1843**, 182-196, doi:10.1016/j.bbamcr.2013.06.031 (2014).
- 6 Uversky, V. N. & Fink, A. L. Conformational constraints for amyloid fibrillation: the importance of being unfolded. *Biochimica et biophysica acta* **1698**, 131-153, doi:10.1016/j.bbapap.2003.12.008 (2004).
- 7 Chiti, F. & Dobson, C. M. Protein misfolding, functional amyloid, and human disease. *Annual review of biochemistry* **75**, 333-366 (2006).
- 8 Eisenberg, D. & Jucker, M. The amyloid state of proteins in human diseases. *Cell* **148**, 1188-1203, doi:DOI 10.1016/j.cell.2012.02.022 (2012).
- 9 Riek, R. & Eisenberg, D. S. The activities of amyloids from a structural perspective. *Nature* **539**, 227, doi:10.1038/nature20416 (2016).
- 10 Greenwald, J. & Riek, R. Biology of amyloid: structure, function, and regulation. *Structure (London, England : 1993)* **18**, 1244-1260, doi:10.1016/j.str.2010.08.009

- (2010).
- 11 Sadigh-Eteghad, S. *et al.* Amyloid-beta: a crucial factor in Alzheimer's disease. *Medical principles and practice : international journal of the Kuwait University, Health Science Centre* **24**, 1-10, doi:10.1159/000369101 (2015).
  - 12 Tycko, R. Physical and structural basis for polymorphism in amyloid fibrils. *Protein Science : A Publication of the Protein Society* **23**, 1528-1539, doi:10.1002/pro.2544 (2014).
  - 13 Hieronymus, L. & Griffin, S. Role of Amylin in Type 1 and Type 2 Diabetes. *The Diabetes educator* **41**, 47s-56s, doi:10.1177/0145721715607642 (2015).
  - 14 Mukherjee, A., Morales-Scheihing, D., Butler, P. C. & Soto, C. Type 2 diabetes as a protein misfolding disease. *Trends in molecular medicine* **21**, 439-449, doi:10.1016/j.molmed.2015.04.005 (2015).
  - 15 Knowles, T. P. J., Vendruscolo, M. & Dobson, C. M. The amyloid state and its association with protein misfolding diseases. *Nature Reviews Molecular Cell Biology* **15**, 384, doi:10.1038/nrm3810 (2014).
  - 16 Stefani, M. & Dobson, C. M. Protein aggregation and aggregate toxicity: new insights into protein folding, misfolding diseases and biological evolution. *Journal of molecular medicine (Berlin, Germany)* **81**, 678-699, doi:10.1007/s00109-003-0464-5 (2003).
  - 17 Li, C. & Mezzenga, R. The interplay between carbon nanomaterials and amyloid fibrils in bio-nanotechnology. *Nanoscale* **5**, 6207-6218, doi:10.1039/c3nr01644g (2013).
  - 18 Romero, D. & Kolter, R. Functional amyloids in bacteria. *International microbiology : the official journal of the Spanish Society for Microbiology* **17**, 65-

- 73, doi:10.2436/20.1501.01.208 (2014).
- 19 Morris, A. M., Watzky, M. A. & Finke, R. G. Protein aggregation kinetics, mechanism, and curve-fitting: a review of the literature. *Biochim. Biophys. Acta* **1794**, 375-397, doi:S1570-9639(08)00348-8 [pii] 10.1016/j.bbapap.2008.10.016 (2009).
- 20 Arosio, P., Knowles, T. P. & Linse, S. On the lag phase in amyloid fibril formation. *Physical chemistry chemical physics : PCCP* **17**, 7606-7618, doi:10.1039/c4cp05563b (2015).
- 21 Jarrett, J. T. & Lansbury, P. T., Jr. Seeding "one-dimensional crystallization" of amyloid: a pathogenic mechanism in Alzheimer's disease and scrapie? *Cell* **73**, 1055-1058, doi:0092-8674(93)90635-4 [pii] (1993).
- 22 Naiki, H., Higuchi, K., Hosokawa, M. & Takeda, T. Fluorometric determination of amyloid fibrils in vitro using the fluorescent dye, thioflavin T1. *Analytical biochemistry* **177**, 244-249 (1989).
- 23 Frid, P., Anisimov, S. V. & Popovic, N. Congo red and protein aggregation in neurodegenerative diseases. *Brain research reviews* **53**, 135-160, doi:10.1016/j.brainresrev.2006.08.001 (2007).
- 24 Ecroyd, H. & Carver, J. A. Crystallin proteins and amyloid fibrils. *Cellular and molecular life sciences : CMLS* **66**, 62-81, doi:10.1007/s00018-008-8327-4 (2009).
- 25 Stranks, S. D. *et al.* Model for amorphous aggregation processes. *Physical review. E, Statistical, nonlinear, and soft matter physics* **80**, 051907, doi:10.1103/PhysRevE.80.051907 (2009).
- 26 Uversky, V. N. Mysterious oligomerization of the amyloidogenic proteins. *The*

- FEBS journal* **277**, 2940-2953, doi:10.1111/j.1742-4658.2010.07721.x (2010).
- 27 Khan, J. M. *et al.* SDS can be utilized as an amyloid inducer: a case study on diverse proteins. *PloS one* **7**, e29694, doi:10.1371/journal.pone.0029694 (2012).
- 28 Ishtikhar, M. *et al.* Rosin Surfactant QRMAE Can Be Utilized as an Amorphous Aggregate Inducer: A Case Study of Mammalian Serum Albumin. *PloS one* **10**, e0139027, doi:10.1371/journal.pone.0139027 (2015).
- 29 Peterson, P. A., Cunningham, B. A., Berggård, I. & Edelman, G. M.  $\beta(2)$ -Microglobulin—A Free Immunoglobulin Domain. *Proceedings of the National Academy of Sciences of the United States of America* **69**, 1697-1701 (1972).
- 30 Trinh, C. H., Smith, D. P., Kalverda, A. P., Phillips, S. E. & Radford, S. E. Crystal structure of monomeric human beta-2-microglobulin reveals clues to its amyloidogenic properties. *Proceedings of the National Academy of Sciences of the United States of America* **99**, 9771-9776, doi:10.1073/pnas.152337399 (2002).
- 31 Iwata, K., Matsuura, T., Sakurai, K., Nakagawa, A. & Goto, Y. High-resolution crystal structure of beta2-microglobulin formed at pH 7.0. *Journal of biochemistry* **142**, 413-419, doi:10.1093/jb/mvm148 (2007).
- 32 Koch, K. M. Dialysis-related amyloidosis. *Kidney international* **41**, 1416-1429 (1992).
- 33 Gejyo, F. *et al.* A new form of amyloid protein associated with chronic hemodialysis was identified as beta 2-microglobulin. *Biochemical and biophysical research communications* **129**, 701-706 (1985).
- 34 Yamamoto, S. & Gejyo, F. Historical background and clinical treatment of dialysis-related amyloidosis. *Biochimica et Biophysica Acta (BBA) - Proteins and Proteomics* **1753**, 4-10, doi:https://doi.org/10.1016/j.bbapap.2005.09.006 (2005).

- 35 Eichner, T. & Radford, S. E. Understanding the complex mechanisms of beta2-microglobulin amyloid assembly. *The FEBS journal* **278**, 3868-3883, doi:10.1111/j.1742-4658.2011.08186.x (2011).
- 36 Ohhashi, Y. *et al.* The intrachain disulfide bond of beta(2)-microglobulin is not essential for the immunoglobulin fold at neutral pH, but is essential for amyloid fibril formation at acidic pH. *Journal of biochemistry* **131**, 45-52 (2002).
- 37 Yamamoto, S. *et al.* Kinetic analysis of the polymerization and depolymerization of  $\beta$ 2-microglobulin-related amyloid fibrils in vitro. *Biochimica et Biophysica Acta (BBA) - Proteins and Proteomics* **1753**, 34-43, doi:https://doi.org/10.1016/j.bbapap.2005.07.007 (2005).
- 38 Kad, N. M., Thomson, N. H., Smith, D. P., Smith, D. A. & Radford, S. E. Beta(2)-microglobulin and its deamidated variant, N17D form amyloid fibrils with a range of morphologies in vitro. *J Mol Biol* **313**, 559-571, doi:10.1006/jmbi.2001.5071 (2001).
- 39 Yanagi, K. *et al.* The Monomer–Seed Interaction Mechanism in the Formation of the  $\beta$ 2-Microglobulin Amyloid Fibril Clarified by Solution NMR Techniques. *Journal of Molecular Biology* **422**, 390-402, doi:https://doi.org/10.1016/j.jmb.2012.05.034 (2012).
- 40 Platt, G. W., Routledge, K. E., Homans, S. W. & Radford, S. E. Fibril growth kinetics reveal a region of beta2-microglobulin important for nucleation and elongation of aggregation. *J. Mol. Biol.* **378**, 251-263, doi:S0022-2836(08)00168-X [pii] 10.1016/j.jmb.2008.01.092 (2008).
- 41 Giehm, L. & Otzen, D. E. Strategies to increase the reproducibility of protein

- fibrillization in plate reader assays. *Anal. Biochem.* **400**, 270-281, doi:Doi 10.1016/J.Ab.2010.02.001 (2010).
- 42 Chatani, E. *et al.* Ultrasonication-dependent production and breakdown lead to minimum-sized amyloid fibrils. *P Natl Acad Sci USA* **106**, 11119-11124, doi:DOI 10.1073/pnas.0901422106 (2009).
- 43 Yoshimura, Y. *et al.* Distinguishing crystal-like amyloid fibrils and glass-like amorphous aggregates from their kinetics of formation. *P Natl Acad Sci USA* **109**, 14446-14451, doi:DOI 10.1073/pnas.1208228109 (2012).
- 44 So, M. *et al.* Ultrasonication-dependent acceleration of amyloid fibril formation. *J. Mol. Biol.* **412**, 568-577, doi:S0022-2836(11)00847-3 [pii] 10.1016/j.jmb.2011.07.069 (2011).
- 45 Liu, T. H. *et al.* Femtosecond-Laser-Enhanced Amyloid Fibril Formation of Insulin. *Langmuir* **33**, 8311-8318, doi:10.1021/acs.langmuir.7b01822 (2017).
- 46 Raman, B. *et al.* Critical balance of charge interactions is required for beta2-microglobulin amyloid fibril growth and stability: influence by co-solute anions. *Biochemistry* **44**, 1288-1299 (2004).
- 47 Yamamoto, S. *et al.* Low concentrations of sodium dodecyl sulfate induce the extension of beta 2-microglobulin-related amyloid fibrils at a neutral pH. *Biochemistry* **43**, 11075-11082, doi:10.1021/bi049262u (2004).
- 48 So, M. *et al.* Supersaturation-Limited and Unlimited Phase Spaces Compete to Produce Maximal Amyloid Fibrillation near the Critical Micelle Concentration of Sodium Dodecyl Sulfate. *Langmuir* **31**, 9973-9982, doi:10.1021/acs.langmuir.5b02186 (2015).
- 49 Yamamoto, S. *et al.* Glycosaminoglycans enhance the trifluoroethanol-induced

- extension of beta 2-microglobulin-related amyloid fibrils at a neutral pH. *Journal of the American Society of Nephrology : JASN* **15**, 126-133 (2004).
- 50 Chatani, E., Yagi, H., Naiki, H. & Goto, Y. Polymorphism of beta2-microglobulin amyloid fibrils manifested by ultrasonication-enhanced fibril formation in trifluoroethanol. *The Journal of biological chemistry* **287**, 22827-22837, doi:10.1074/jbc.M111.333310 (2012).
- 51 Tycko, R. & Wickner, R. B. Molecular structures of amyloid and prion fibrils: consensus versus controversy. *Acc. Chem. Res.* **46**, 1487-1496, doi:10.1021/ar300282r (2013).
- 52 Sipe, J. D. *et al.* Amyloid fibril protein nomenclature: 2012 recommendations from the Nomenclature Committee of the International Society of Amyloidosis. *Amyloid* **19**, 167-170, doi:10.3109/13506129.2012.734345 (2012).
- 53 Wetzel, R. Kinetics and thermodynamics of amyloid fibril assembly. *Acc. Chem. Res.* **39**, 671-679, doi:10.1021/ar050069h (2006).
- 54 Kitayama, H. *et al.* A common mechanism underlying amyloid fibrillation and protein crystallization revealed by the effects of ultrasonication. *Biochim. Biophys. Acta* **1834**, 2640-2646, doi:S1570-9639(13)00350-6 [pii] 10.1016/j.bbapap.2013.09.016 (2013).
- 55 Lin, Y., Lee, Y. H., Yoshimura, Y., Yagi, H. & Goto, Y. Solubility and supersaturation-dependent protein misfolding revealed by ultrasonication. *Langmuir* **30**, 1845-1854, doi:10.1021/la403100h (2013).
- 56 Muta, H. *et al.* Supersaturation-limited amyloid fibrillation of insulin revealed by ultrasonication. *J. Biol. Chem.* **289**, 18228-18238, doi:M114.566950 [pii] 10.1074/jbc.M114.566950 (2014).

- 57 Ikenoue, T. *et al.* Heat of supersaturation-limited amyloid burst directly monitored by isothermal titration calorimetry. *Proc Natl Acad Sci USA* **111**, 6654-6659, doi:1322602111 [pii] 10.1073/pnas.1322602111 (2014).
- 58 Hofrichter, J., Ross, P. D. & Eaton, W. A. Supersaturation in sickle cell hemoglobin solutions. *P Natl Acad Sci USA* **73**, 3035-3039 (1976).
- 59 Eaton, W. A. & Hofrichter, J. Hemoglobin S gelation and sickle cell disease. *Blood* **70**, 1245-1266 (1987).
- 60 Ciryam, P., Tartaglia, G. G., Morimoto, R. I., Dobson, C. M. & Vendruscolo, M. Widespread aggregation and neurodegenerative diseases are associated with supersaturated proteins. *Cell Rep* **5**, 781-790, doi:DOI 10.1016/j.celrep.2013.09.043 (2013).
- 61 Bemporad, F. & Chiti, F. Protein misfolded oligomers: experimental approaches, mechanism of formation, and structure-toxicity relationships. *Chemistry & biology* **19**, 315-327, doi:10.1016/j.chembiol.2012.02.003 (2012).
- 62 Miti, T., Mulaj, M., Schmit, J. D. & Muschol, M. Stable, metastable, and kinetically trapped amyloid aggregate phases. *Biomacromol.* **16**, 326-335, doi:10.1021/bm501521r (2015).
- 63 Ohhashi, Y., Kihara, M., Naiki, H. & Goto, Y. Ultrasonication-induced amyloid fibril formation of beta2-microglobulin. *J. Biol. Chem.* **280**, 32843-32848 (2005).
- 64 Yoshimura, Y., So, M., Yagi, H. & Goto, Y. Ultrasonication: an efficient agitation for accelerating the supersaturation-limited amyloid fibrillation of proteins. *Jap. J. App. Phys.* **52**, 01-08 (2013).
- 65 Yamaguchi, K., Matsumoto, T. & Kuwata, K. Proper calibration of ultrasonic

- power enabled the quantitative analysis of the ultrasonication-induced amyloid formation process. *Protein Sci.* **21**, 38-49 (2012).
- 66 Umemoto, A., Yagi, H., So, M. & Goto, Y. High-throughput analysis of the ultrasonication-forced amyloid fibrillation reveals the mechanism underlying the large fluctuation in the lag time. *J. Biol. Chem.* **289**, 27290-27299 doi:M114.569814 [pii]  
10.1074/jbc.M114.569814 (2014).
- 67 Yagi, H., Hasegawa, K., Yoshimura, Y. & Goto, Y. Acceleration of the depolymerization of amyloid beta fibrils by ultrasonication. *Biochim. Biophys. Acta* **1834**, 2480-2485, doi:S1570-9639(13)00311-7 [pii]  
10.1016/j.bbapap.2013.08.013 (2013).
- 68 Yagi, H. *et al.* Ultrasonication-dependent formation and degradation of alpha-synuclein amyloid fibrils. *Biochimica et biophysica acta* **1854**, 209-217, doi:S1570-9639(14)00330-6 [pii]  
10.1016/j.bbapap.2014.12.014 (2014).
- 69 Adachi, M., So, M., Sakurai, K., Kardos, J. & Goto, Y. Supersaturation-limited and Unlimited Phase Transitions Compete to Produce the Pathway Complexity in Amyloid Fibrillation. *The Journal of biological chemistry* **290**, 18134-18145, doi:10.1074/jbc.M115.648139 (2015).
- 70 Chiba, T. *et al.* Amyloid fibril formation in the context of full-length protein: effects of proline mutations on the amyloid fibril formation of beta2-microglobulin. *J. Biol. Chem.* **278**, 47016-47024 (2003).
- 71 Kardos, J. *et al.* Structural studies reveal that the diverse morphology of  $\beta$ 2-microglobulin aggregates is a reflection of different molecular architectures.

- Biochimica et Biophysica Acta (BBA) - Proteins and Proteomics* **1753**, 108-120, doi:<https://doi.org/10.1016/j.bbapap.2005.08.013> (2005).
- 72 Bouchard, M., Zurdo, J., Nettleton, E. J., Dobson, C. M. & Robinson, C. V. Formation of insulin amyloid fibrils followed by FTIR simultaneously with CD and electron microscopy. *Protein Science : A Publication of the Protein Society* **9**, 1960-1967 (2000).
- 73 Goto, Y. & Fink, A. L. Conformational state of beta-lactamase: Molten-globule states at acidic and alkaline pH with high salt. *Biochemistry* **28**, 945-952 (1988).
- 74 Bramanti, E., Fulgentini, L., Bizzarri, R., Lenci, F. & Sgarbossa, A.  *$\beta$ -Amyloid Amorphous Aggregates Induced by the Small Natural Molecule Ferulic Acid*. Vol. 117 (2013).
- 75 Arosio, P. *et al.* In Vitro Aggregation Behavior of a Non-Amyloidogenic  $\lambda$  Light Chain Dimer Deriving from U266 Multiple Myeloma Cells. *PloS one* **7**, e33372, doi:[10.1371/journal.pone.0033372](https://doi.org/10.1371/journal.pone.0033372) (2012).
- 76 Souillac, P. O. *et al.* Elucidation of the molecular mechanism during the early events in immunoglobulin light chain amyloid fibrillation - Evidence for an off-pathway oligomer at acidic pH. *J. Biol. Chem.* **277**, 12666-12679, doi:[DOI 10.1074/jbc.M109229200](https://doi.org/10.1074/jbc.M109229200) (2002).
- 77 Souillac, P. O., Uversky, V. N. & Fink, A. L. Structural transformations of oligomeric intermediates in the fibrillation of the immunoglobulin light chain LEN. *Biochemistry* **42**, 8094-8104, doi:[Doi 10.1021/Bi034652m](https://doi.org/10.1021/Bi034652m) (2003).
- 78 Gosal, W. S. *et al.* Competing pathways determine fibril morphology in the self-assembly of beta(2)-microglobulin into amyloid. *J. Mol. Biol.* **351**, 850-864, doi:[DOI 10.1016/j.jmb.2005.06.040](https://doi.org/10.1016/j.jmb.2005.06.040) (2005).

- 79 Hong, D. P., Ahmad, A. & Fink, A. L. Fibrillation of human insulin A and B chains. *Biochemistry* **45**, 9342-9353, doi:Doi 10.1021/Bi0604936 (2006).
- 80 Dusa, A. *et al.* Characterization of oligomers during alpha-synuclein aggregation using intrinsic tryptophan fluorescence. *Biochemistry* **45**, 2752-2760, doi:10.1021/bi051426z (2006).
- 81 Uversky, V. N. & Eliezer, D. Biophysics of parkinson's disease: structure and aggregation of alpha-synuclein. *Curr Protein Pept Sc* **10**, 483-499 (2009).
- 82 Hall, D., Kardos, J., Edskes, H., Carver, J. A. & Goto, Y. A multi-pathway perspective on protein aggregation: Implications for control of the rate and extent of amyloid formation. *FEBS Lett.*, Published online: January 31, 2015, doi:S0014-5793(15)00061-7 [pii] 10.1016/j.febslet.2015.01.032 (2015).
- 83 Sasahara, K., Yagi, H., Naiki, H. & Goto, Y. Heat-induced conversion of beta(2)-microglobulin and hen egg-white lysozyme into amyloid fibrils. *J. Mol. Biol.* **372**, 981-991, doi:S0022-2836(07)00896-0 [pii] 10.1016/j.jmb.2007.06.088 (2007).
- 84 Sasahara, K., Yagi, H., Sakai, M., Naiki, H. & Goto, Y. Amyloid nucleation triggered by agitation of beta(2)-microglobulin under acidic and neutral pH conditions. *Biochemistry* **47**, 2650-2660, doi:Doi 10.1021/Bi701968g (2008).
- 85 Korevaar, P. A. *et al.* Pathway complexity in supramolecular polymerization. *Nature* **481**, 492-496, doi:Doi 10.1038/Nature10720 (2012).
- 86 Kardos, J., Yamamoto, K., Hasegawa, K., Naiki, H. & Goto, Y. Direct measurement of the thermodynamic parameters of amyloid formation by isothermal titration calorimetry. *J. Biol. Chem.* **279**, 55308-55314, doi:DOI

- 10.1074/jbc.M409677200 (2004).
- 87 Kardos, J. *et al.* Reversible heat-induced dissociation of beta2-microglobulin amyloid fibrils. *Biochemistry* **50**, 3211-3220, doi:10.1021/bi2000017 (2011).
- 88 Wolynes, P. G. Energy landscapes and solved protein-folding problems. *Philos T Roy Soc A* **363**, 453-464, doi:DOI 10.1098/rsta.2004.1502 (2005).
- 89 Bryngelson, J. D., Onuchic, J. N., Socci, N. D. & Wolynes, P. G. Funnels, pathways, and the energy landscape of protein folding: a synthesis. *Proteins* **21**, 167-195, doi:DOI 10.1002/prot.340210302 (1995).
- 90 Nymeyer, H., Garcia, A. E. & Onuchic, J. N. Folding funnels and frustration in off-lattice minimalist protein landscapes. *P Natl Acad Sci USA* **95**, 5921-5928, doi:DOI 10.1073/pnas.95.11.5921 (1998).
- 91 Roberts, C. J. Therapeutic protein aggregation: mechanisms, design, and control. *Trends in biotechnology* **32**, 372-380, doi:10.1016/j.tibtech.2014.05.005 (2014).
- 92 Singh, J. & Udgaonkar, J. B. Molecular Mechanism of the Misfolding and Oligomerization of the Prion Protein: Current Understanding and Its Implications. *Biochemistry* **54**, 4431-4442, doi:10.1021/acs.biochem.5b00605 (2015).
- 93 Arosio, P., Vendruscolo, M., Dobson, C. M. & Knowles, T. P. Chemical kinetics for drug discovery to combat protein aggregation diseases. *Trends in pharmacological sciences* **35**, 127-135, doi:10.1016/j.tips.2013.12.005 (2014).
- 94 Sasahara, K., Naiki, H. & Goto, Y. Kinetically controlled thermal response of beta2-microglobulin amyloid fibrils. *J Mol Biol* **352**, 700-711, doi:10.1016/j.jmb.2005.07.033 (2005).
- 95 Sasahara, K., Yagi, H., Naiki, H. & Goto, Y. Thermal Response with Exothermic Effects of  $\beta$ 2-Microglobulin Amyloid Fibrils and Fibrillation. *Journal of*

- Molecular Biology* **389**, 584-594, doi:<https://doi.org/10.1016/j.jmb.2009.04.026> (2009).
- 96 Ikenoue, T. *et al.* Cold denaturation of alpha-synuclein amyloid fibrils. *Angewandte Chemie (International ed. in English)* **53**, 7799-7804, doi:[10.1002/anie.201403815](https://doi.org/10.1002/anie.201403815) (2014).
- 97 Sanfelice, D. & Temussi, P. A. Cold denaturation as a tool to measure protein stability. *Biophysical chemistry* **208**, 4-8, doi:[10.1016/j.bpc.2015.05.007](https://doi.org/10.1016/j.bpc.2015.05.007) (2016).
- 98 Dobson, C. M. Protein misfolding, evolution and disease. *Trends in Biochemical Sciences* **24**, 329-332, doi:[https://doi.org/10.1016/S0968-0004\(99\)01445-0](https://doi.org/10.1016/S0968-0004(99)01445-0) (1999).
- 99 Greene, D. G., Modla, S., Wagner, N. J., Sandler, S. I. & Lenhoff, A. M. Local Crystalline Structure in an Amorphous Protein Dense Phase. *Biophysical journal* **109**, 1716-1723, doi:[10.1016/j.bpj.2015.08.023](https://doi.org/10.1016/j.bpj.2015.08.023) (2015).
- 100 Ng, J. D. *et al.* The crystallization of biological macromolecules from precipitates: evidence for Ostwald ripening. *Journal of Crystal Growth* **168**, 50-62, doi:[https://doi.org/10.1016/0022-0248\(96\)00362-4](https://doi.org/10.1016/0022-0248(96)00362-4) (1996).

## List of publications

### *Main paper*

Adachi, M., So, M., Sakurai, K., Kardos, J., and Goto, Y.

**Supersaturation-limited and Unlimited Phase Transitions Compete to Produce the Pathway Complexity in Amyloid Fibrillation.**

*The Journal of biological chemistry* **290**, 18134-18145 (2015).

Adachi, M., So, M., Goto, Y.

**Comprehensive understanding of heat- and salt-dependent protein aggregation based on the supersaturation-limited competitive mechanism.**

*In preparation*

### *Collaborations*

Terakawa, M. S., Yagi, H., Adachi, M., Lee, Y. H., and Goto, Y.

**Small liposomes accelerate the fibrillation of amyloid beta (1-40).**

*The Journal of biological chemistry* **290**, 815-826 (2015)

Yagi, H., Mizuno, A., So, M., Hirano, M., Adachi, M., Akazawa-Ogawa, Y., Hagihara, Y.,

Ikenoue, T., Lee, Y. H., Kawata, Y., and Goto, Y.

**Ultrasonication-dependent formation and degradation of alpha-synuclein amyloid fibrils.**

*Biochimica et biophysica acta* **1854**, 209-217 (2015)

Ida, M., Ando, M., Adachi, M., Tanaka, A., Machida, K., Hongo, K., Mizobata, T., Yamakawa, M. Y., Watanabe, Y., Nakashima, K., and Kawata, Y.

**Structural basis of Cu, Zn-superoxide dismutase amyloid fibril formation involves interaction of multiple peptide core regions.**

*Journal of biochemistry* **159**, 247-260 (2016)

Noda, S., So, M., Adachi, M., Kardos, J., Akazawa-Ogawa, Y., Hagihara, Y., and Goto, Y.

**Thioflavin T-Silent Denaturation Intermediates Support the Main-Chain-Dominated Architecture of Amyloid Fibrils.**

*Biochemistry* **55**, 3937-3948 (2016)

Hall, D., Zhao, R., So, M., Adachi, M., Rivas, G., Carver, J. A., and Goto, Y.

**Recognizing and analyzing variability in amyloid formation kinetics: Simulation and statistical methods.**

*Analytical biochemistry* **510**, 56-71 (2016)

Nitani, A.<sup>1</sup>, Muta, H.<sup>1</sup>, Adachi, M.<sup>1</sup>, So, M., Sasahara, K., Sakurai, K., Chatani, E., Naoe, K., Ogi, H., Hall, D., and Goto, Y.

**Heparin-dependent aggregation of hen egg white lysozyme reveals two distinct mechanisms of amyloid fibrillation.**

*The Journal of biological chemistry* (2017)

<sup>1</sup>These authors contributed equally to this work.

Goto, Y., Adachi, M., Muta, H. & So, M.

**Salt-induced formations of partially folded intermediates and amyloid fibrils suggests a common underlying mechanism.**

*Biophysical reviews*, doi:10.1007/s12551-017-0370-7 (2017)